

The variety of cytosolic calcium responses and possible roles of PLC and PKC

Minchul Kang¹ and Hans G Othmer²

¹ Departments of Molecular Physiology and Biophysics, Vanderbilt University School of Medicine, Nashville, TN 37232, USA

² School of Mathematics, University of Minnesota, Minneapolis, MN 55455, USA

E-mail: minchul.kang@vanderbilt.edu and othmer@math.umn.edu

Received 27 August 2007

Accepted for publication 22 November 2007

Published 13 December 2007

Online at stacks.iop.org/PhysBio/4/325

Abstract

A model of ligand-induced intracellular calcium (Ca^{2+}) responses incorporating phospholipase C (PLC) and protein kinase C (PKC) is developed for the purpose of understanding the mechanisms underlying the observed temporal patterns of intracellular calcium (Ca_i^{2+}) under sustained agonist stimulation. Some studies have suggested that inhibition of ligand receptors and PLC by PKC could generate sinusoidal Ca^{2+} oscillations, while PKC-independent Ca^{2+} -induced Ca^{2+} release (CICR) via IP_3 -gated Ca^{2+} channels on the endoplasmic reticulum (ER) is believed to be responsible for baseline spiking. However, some evidence also indicates that baseline spiking can be observed under high-PKC activity, or under low-PKC activity with low agonist stimulus, as well. Insight into the basis of these observations regarding the role of PKC in Ca_i^{2+} response patterns can be gained by developing and analyzing a mathematical model of Ca_i^{2+} responses. We do this herein and find that (1) interaction of CICR and the sarcoplasmic/endoplasmic reticulum calcium ATPase (SERCA) pump is enough to generate both types of Ca_i^{2+} oscillations, (2) there exist four possible Ca_i^{2+} response patterns under sustained agonist stimulus: a sub-threshold response (SR), baseline spiking, sinusoidal oscillations (SO) and transient with plateau, and (3) the IP_3 concentration, which is controlled by the strength of the interaction between PKC and PLC, can be used to predict the Ca_i^{2+} response patterns. From this analysis we conclude that the different patterns of Ca_i^{2+} oscillations can be understood as a generic consequence of the interactions between CICR via the IP_3 -gated Ca^{2+} channels in response to changes in the level of IP_3 , and re-uptake into the ER/SR via the SERCA pump. PKC, in conjunction with PLC, can act as a switch between different Ca_i^{2+} response patterns by modulating the cytosolic IP_3 level, which determines the Ca_i^{2+} patterns.

1. Introduction

Ca^{2+} participates in many biological signal transduction pathways and the processes they control, including enzyme activation, endo- and exocytosis, chemotaxis, vesicle-mediated release of various molecules, and fertilization [4]. The basal cytoplasmic Ca^{2+} concentration is kept quite low (20–100 nM) while the extracellular concentration and the concentration in intracellular stores is high (~1 mM) [3], which facilitates rapid cytosolic increases. The extremely low concentrations of intracellular Ca^{2+} are believed to be important not only because high- Ca^{2+} intracellular

concentrations are toxic to cells, but also because Ca^{2+} is a very potent cellular messenger. Since it cannot be degraded, cells regulate the intracellular Ca^{2+} concentration ($[\text{Ca}_i^{2+}]$) closely by complexing it with proteins, by compartmentalization, and by active removal from the cells. Less than 1% of the total Ca_i^{2+} exists in the free ionized form at steady state [3]; the remainder is predominantly sequestered in the endoplasmic reticulum (ER) and sarcoplasmic reticulum (SR), with smaller amounts stored in the mitochondria and the nucleus [92]. Intracellular Ca^{2+} is closely regulated by balancing efflux from the ER via IP_3 -gated channels against Ca^{2+} transport into the ER by the SERCA pump. When Ca^{2+} homeostasis mechanisms

Table 1. A comparison of the two modes of oscillation.

	Baseline Ca^{2+} spiking	Sinusoidal Ca^{2+} oscillation	Reference
Other names	Regenerative CICR [57] Spike-type	Dynamic uncoupling [57] PLC/PKC oscillation [66] Continuous-type	[57] [80]
Frequency	Low $< 1 \text{ min}^{-1}$ Frequency \propto agonist concentration Frequency \propto PLC activity Frequency \propto IP_3 concentration	High $> 1 \text{ min}^{-1}$ Independent of agonist concentration Independent of PLC activity Independent of IP_3 concentration	[88] [57, 66, 88] [57]
Amplitude	Relatively constant Independent of agonist concentration	Decrease in time Amplitude \propto agonist concentration	[88] [88]
Trace property	Come down to basal level Maintain the same amplitudes	Sustained level of Ca^{2+} oscillation Oscillation diminish at time	[88, 80]
IP_3 level	Low	High	[22]
Agonist	Low	High	[57, 100]
PLC activity	Low	High	
PKC activity	High	Low	[57, 100]
Feedback	Ca^{2+} [100]	PKC [8]	[57]
Latency	Long (agonist dependent)	Short	[88]
Typical receptor	mGluR ₅ , P2Y CaR Noradrenergic α_{1B} Cholecystokinin	mGluR ₅ , P2Y Noradrenergic α_{1B} Acetylcholine	[57] [101] [100] [48]

are perturbed by agonists which activate G-protein-coupled receptors (GPCRs), the $[\text{Ca}_i^{2+}]$ rises after a delay of 5–10 s from a resting value of 100 nM to a peak value of 400–800 nM [74]. However, the characteristics of the Ca_i^{2+} response patterns vary from one cell type to another, and it has been suggested that not only the cell type, but also the type of agonists and/or the phenotype of the cells (fresh/cultured) could be responsible for different Ca_i^{2+} response patterns [48, 74]. The transduced signal information may be encoded by the frequency, amplitude and duration of the signal, as well as by combinations of them [19, 44, 49, 77, 82]. Typically cells display cell-specific response characteristics depending on the strength and/or types of stimuli [60, 72, 73, 88]. In addition, the Ca_i^{2+} response patterns display a variety of temporal characteristics, such as smooth oscillations, bursting (a periodic succession of quiescent and active phases) or chaotic oscillations [10, 23, 26, 35, 45, 76]. When spatial variations of the signal or downstream components are present as well, the result may be complex spatio-temporal patterns of Ca_i^{2+} response [10, 23, 26, 45, 76].

Despite the diversity of the Ca_i^{2+} responses, cells preserve their cell-specific pattern of Ca^{2+} spiking or oscillations, which is called the intracellular Ca^{2+} fingerprint [65], under similar physiological conditions [40, 65, 72]. Two major types of intracellular Ca^{2+} oscillation patterns stand out from the possible fingerprints; these are known as baseline Ca^{2+} spiking (BLS) and sinusoidal Ca^{2+} oscillations (SO). BLS is characterized by low-frequency ($< 1 \text{ min}^{-1}$) Ca_i^{2+} oscillations initiated from a baseline of Ca_i^{2+} that is close to the resting Ca^{2+} level and can be maintained for relatively long periods between individual Ca_i^{2+} spikes, whereas SO is characterized by high-frequency ($> 1 \text{ min}^{-1}$) symmetrical oscillations superimposed on an elevated level of Ca_i^{2+} [72, 74, 88]. A more detailed

comparison between these Ca^{2+} oscillation patterns is given in table 1.

Unlike the oscillatory responses, two types of non-oscillatory responses (SR and TP) have received less attention. While the oscillatory Ca^{2+} responses are observed at intermediate IP_3 levels, SR or RP are observed under low- or high- IP_3 levels, respectively. In dynamical systems terms, SR can be understood as a subthreshold response of an excitable system, while TP reflects the presence of bistability. In more biological terms, SR could be related to blips and puffs which do not develop into global events such as Ca_i^{2+} oscillation or/and waves [26, 90], while TP could reflect a situation in which the ER lumen is depleted following release of most of the Ca^{2+} [53, 96].

A large body of evidence indicates an important role for PKC in Ca_i^{2+} responses [1, 31, 47, 85, 93, 94]. Moreover, several studies indicate that inhibition of (GPCRs) and/or PLC by PKC is involved in SO [8, 14, 41, 55, 57, 66–68], while a PKC-independent CICR mechanism generates BLS [2, 57, 67]. However there is contradictory evidence which suggests that BLS arises under high-PKC activity [55, 101] as well as at low PKC [57]. More puzzling is that $[\text{Ca}_i^{2+}]$ oscillations can disappear when PKC activity is blocked, but reappears when agonist concentration is lowered [57].

To shed light on the role of PKC in Ca_i^{2+} response patterns, we develop and analyze a deterministic model of glutamate-induced Ca^{2+} oscillations in astrocytes stimulated with constant agonist levels. We choose this as a model system because it involves signal transduction mediated by GPCRs and includes all the downstream components involved in Ca^{2+} release and feedback to receptors [14, 54]. Although other ligand and their corresponding receptors may have different kinetic properties, they will show qualitatively similar

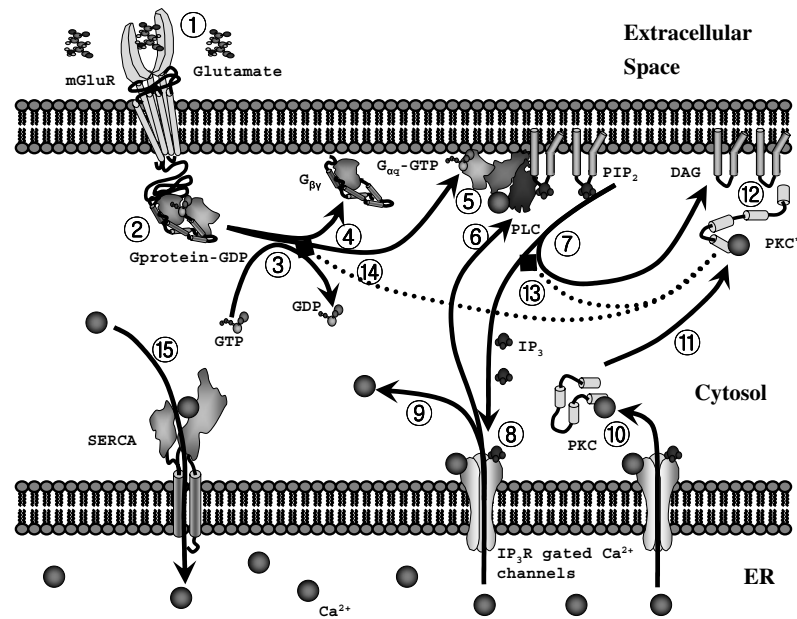


Figure 1. The glutamate-induced Ca_i^{2+} signaling pathway. (1) Glutamate binds to mGluR. (2) G-protein binds to glutamate-mGluR complex. (3) GDP in the G-protein is exchanged for GTP. (4) The G-protein splits into the G_α subunit and $\beta\gamma$ subunit. (5) The $G_\alpha q$ subunit of G-protein binds to PLC. (6) PLC activity is calcium dependent. (7) PLC produces IP_3 and DAG from PIP_2 . (8) IP_3 binds to 3R on the ER membrane. (9) Ca^{2+} is released from the ER (10) Ca^{2+} binds to PKC. (11) PKC translocates to the membrane. (12) PKC binds to DAG and docks at the membrane. (13) PKC phosphorylates the $G_\alpha q$ -PLC complex. (14) PKC phosphorylates mGluRs. (15) SERCA pumps Ca^{2+} into the ER.

behaviors if they share the same downstream structure of the signaling pathway.

A previous model based on GPCRs and Ca^{2+} signaling, comprising similar component steps, was used for studying autoinhibition of voltage-controlled calcium channels in neurons via a feedback loop triggered by neurotransmitter release [78]. The present model is used to identify the possible basic signaling phonemes in complex Ca^{2+} responses and to analyze their underlying mechanisms in terms of interactions among various cytosolic and membrane-associated proteins. The ligand-induced Ca^{2+} signal transduction network comprises 19 distinct species, and to simplify it we adopt a modular approach in which we split the complex network into independent modules which have their own input and output signals. Of course, the output of one module will be an input to one or more of the other network modules. After studying the component modules and verifying that the input–output characteristics are in a biologically-reasonable range, we reassemble the modules into a model for whole network.

2. The mathematical model

2.1. Overview of the glutamate-stimulated signaling pathway

In cultured hippocampal neurons, the postsynaptic concentration of glutamate in the center of the synapse has been estimated to reach levels of approximately 1 mM [13, 58], and the enzymes activated by glutamate receptors on other neurons or astrocytes produce second

messengers to activate secondary effectors or to act directly on regulatory proteins [15]. For example, when glutamate binds to the metabotropic glutamate receptors (mGluRs) on astrocytes (figure 1—step 1: [58]), the ligand–receptor complex allows a G-protein bearing GDP to bind to an intracellular domain of the receptor (figure 1—step 2: [27]), which facilitates the GDP–GTP exchange (figure 1—step 3: [61]). The GTP bound G-protein then dissociates into $\beta\gamma$ -subunits and a GTP bearing G_α -subunit (figure 1—step 4: [5]). The active G_α -subunit activates PLC (figure 1—step 5: [34]) in a Ca^{2+} -dependent manner (figure 1—step 6: [34]), and the activated PLC produces diacylglycerol (DAG) and IP_3 from phosphatidylinositol 4,5-bisphosphate (PIP_2) on the inner membrane (figure 1—step 7: [52]). The DAG in turn recruits PKC to the membrane and activates it. When bound to PLC, the G_α -subunit becomes inactivated by hydrolysis of GTP to GDP, which leads to dissociation of the G_α -subunit from PLC and reassociation with a $\beta\gamma$ -subunit. This in turn inactivates PLC and terminates production of IP_3 and DAG from PIP_2 [16, 78, 82].

IP_3 serves as a water-soluble, diffusible second messenger, while hydrophobic DAG remains on the membrane. When IP_3 diffuses into the intracellular space and binds to specific receptors on Ca_i^{2+} channels in the ER (figure 1—step 8: [6, 39, 52, 86, 87, 98]), Ca^{2+} is released into the intracellular space (figure 1—step 9: [6, 39, 52, 86, 87, 98]), which can then activate a variety of cellular processes [3]. One of the Ca_i^{2+} targets is PKC (figure 1—step 10: [1, 14, 31, 85, 93, 94]), which is activated by Ca_i^{2+} , DAG and

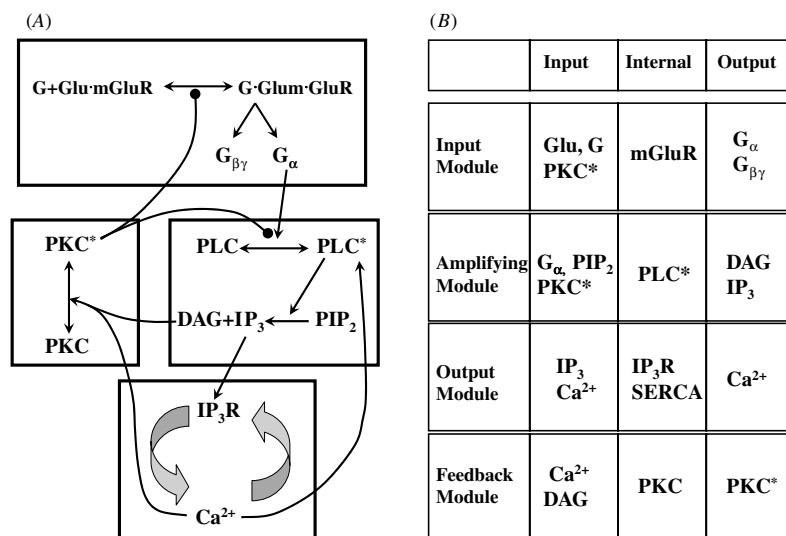


Figure 2. The modular representation of the glutamate-induced Ca^{2+} release pathway. Each box in (A) represents a submodule described in (B). An ‘*’ denotes the activated form of a protein; the column labeled internal in (B) refers to variables that are internal to the module. The description of the modules is given in the text.

membrane phospholipids that exist on the inner leaflet of the plasma membrane (figure 1—step 11: [14, 94, 93]). Activated PKC phosphorylates various membrane-associated and cytoplasmic protein substrates in the cell. For example, it regulates both PLC (figure 1—step 13: [29]) and the G-protein-interacting domain of the mGluR (figure 1—step 14: [30, 41]) by phosphorylation. PLC phosphorylation leads to a decrease of phosphatidylinositide turnover and intracellular Ca_i^{2+} release [102], and the phosphorylation of mGluR reduces the coupling of mGluR and the G-protein activation [30, 41]. Simultaneously, a calcium pump (SERCA) in sarco- or endoplasmic reticulum moves Ca^{2+} from the cytosol into the ER (figure 1—step 15: [24, 63])

2.2. The modular representation of the system

The modular representation of the signaling network is shown in figure 2, and as one sees there, the network can be broken into four interconnected submodules: (i) an input module, (ii) an amplifying module, (iii) an output module, and (iv) a feedback module. The input module receives glutamate and modulatory PKC signals as inputs and produces G_α and $G_{\beta\gamma}$ from G proteins as outputs. Given G_α , PIP₂ and activated PKC as inputs, the amplifying module produces IP₃ and DAG via the action of PLC on PIP₂. The output module comprises the Ca^{2+} handling mechanisms such as IP₃-stimulated release from the ER and SERCA uptake; its inputs are IP₃ and Ca_i^{2+} and the output is Ca_i^{2+} . Finally, the feedback module receives Ca_i^{2+} and DAG as inputs and produces the activated state of PKC, which downregulates the activity of the input module (figure 2). There are a number of negative feedback loops in this network. For instance, at low calcium one loop begins with G_α , and has positive steps through PLC activation, IP₃ production, Ca_i^{2+} release and Ca_i^{2+} -modulated activation of PKC, and a final negative step via PKC* modulation of GPCR. This same loop becomes a positive feedback loop when calcium is high,

for then an increase of IP₃ reduces the rate of Ca_i^{2+} release. Note that there is another, shorter negative feedback loop at low calcium that short-circuits the production of G_α via the inhibitory effect of PKC on PLC activation.

2.3. Kinetic equations

In order to develop a tractable model, several components and processes that may play a role in shaping the Ca^{2+} oscillations are not incorporated. These include (i) glutamate-sensitive AMPA and NMDA channels, (ii) the Ca^{2+} -Na⁺ exchanger on the cell membrane, (iii) the Ca^{2+} kinetics related to mitochondria, and (iv) Ca^{2+} buffers in the cytosol. The capacitive Ca^{2+} currents or store-operated Ca^{2+} entry (SOC) will be treated indirectly by assuming that a Ca^{2+} sensor in the inner-membrane of the ER controls capacitive Ca^{2+} currents to maintain the ER Ca^{2+} concentration constant. There are several detailed models for IP₃-gated channels (3Rs) in the literature [42, 59, 84, 99], but to avoid some of the complexities in these models we will assume that there is only one Ca^{2+} store which is operated by one type of 3R with a biphasic open probability [28]. More detailed models of the ER have been developed [21, 48, 81], but activation of IP₃ receptors by sequential binding of IP₃ and Ca^{2+} seems to fit well with experimental data [59, 99] and we will adopt this sequential binding model for Ca^{2+} release from the ER.

We also restrict attention to a spatially-uniform system in this paper; spatial variations within a cell will be treated elsewhere. We treat the glutamate concentration as a constant and assume that the glutamate receptors, G proteins, PLC, IP₃, DAG, cytosolic Ca^{2+} , IP₃ receptors and PKC are uniformly distributed on or within the cell. The amounts of all membrane-localized components are reported in volumetric concentrations, and mass action kinetics are used for all binding and conversion steps. Stochastic effects are ignored

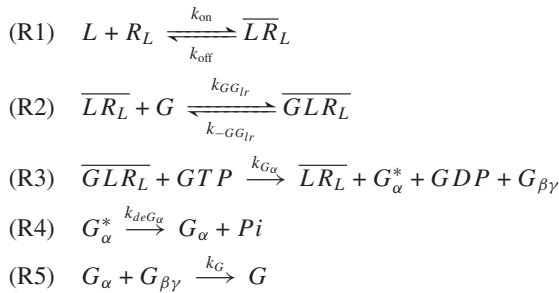
Table 2. Notation for the variables in the model.

Notation	Meaning	Notation	Meaning
L	Glutamate	R_L	Glutamate receptor (mGluR)
$\overline{LR_L}$	Glutamate & Glutamate receptor complex	G	G-protein
$\overline{GLR_L}$	G-protein, glutamate-mGluR complex	G_α	Inactive G_α subunit of G protein
G_α^*	$G_\alpha GTP$	$G_{\beta\gamma}$	$\beta\gamma$ subunit of G protein
GTP	Cytosolic GTP	GDP	cytosolic GDP
P_i	Phosphate	PLC	PLC
$\overline{G_\alpha^* PLC}$	$G_\alpha GTP$, PLC complex	PLC^*	$Ca^{2+} \cdot G_\alpha^* \cdot PLC$ complex (activated state of PLC)
PIP_2	PIP ₂	DAG	DAG
IP_2	Inositol 1,4-bisphosphate	PC	Phosphatidylcholine
Ca^{2+}	Ca^{2+}	PKC	PKC
$\overline{Ca^{2+} PKC}$	$Ca^{2+} \cdot PKC$ complex	$\overline{Ca^{2+} DAG PKC}$	$Ca^{2+} \cdot DAG \cdot PKC$ complex
PKC^*	Activated $Ca^{2+} DAG PKC$	$\overline{PKC^* LR_L}$	PKC^* and $\overline{LR_L}$ complex
$\overline{PLC^* PIP_2}$	PIP ₂ & PLC^* complex	$\overline{PKC^* PLC^*}$	PKC^* & PLC^* complex
IP_3	IP ₃	$\overline{PKC^* PLC^* PIP_2}$	$Ca^{2+} DAG PKC^*$ & $\overline{Ca^{2+} G_\alpha^* PLC PIP_2}$ complex
R_I	IP ₃ receptor (IP ₃ R)	$\overline{IP_3 R_I}$	IP_3 & R_I complex
$\overline{Ca^{2+} IP_3 R_I}$	$\overline{IP_3 R_I}$ & Ca^{2+} complex	$\overline{Ca^{2+} Ca^{2+} IP_3 R_I}$	Ca^{2+} & $\overline{Ca^{2+} IP_3 R_I}$ complex

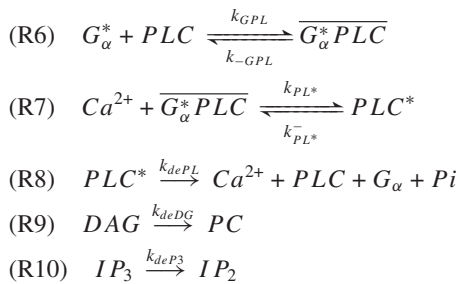
here but may be important in some instances. For simplicity, no isoforms or isozymes of proteins will be considered, even though they may be present. Furthermore, as described in the following section, we simplified the number of reactions and reaction orders based on Codazii *et al* [14, 54], for simplicity (figure 1).

2.3.1. The reaction network. Using the assumptions stated in the preceding sections we can derive the kinetic equations that govern the dynamics. We divide the whole system into four interacting submodules as described earlier, we denote activated states as $*$, a complex of A and B as \overline{AB} , and we use the nomenclature given in table 2.

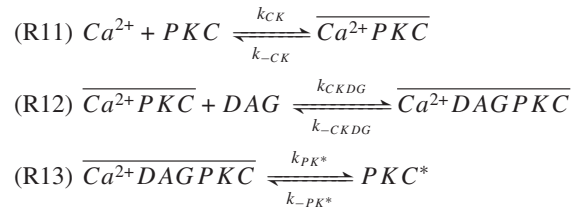
Input.



Amplification.

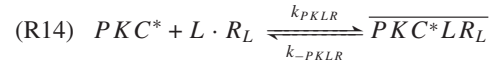


Feedback control–PKC activation kinetics.

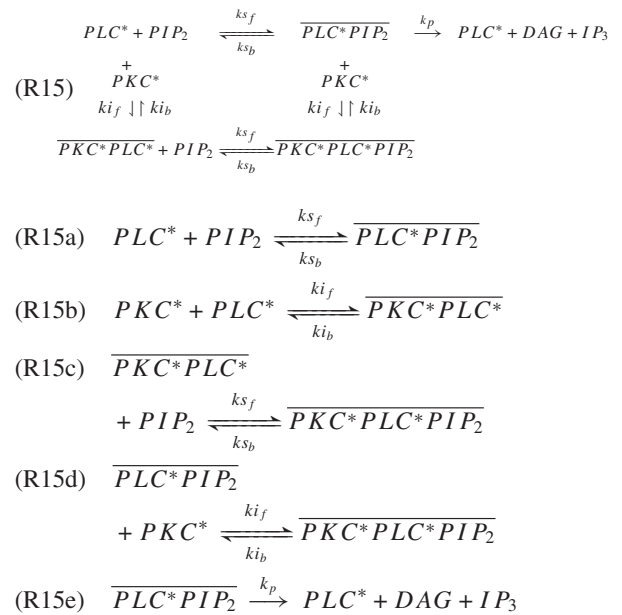


Feedback control–PKC inhibition of PLC and R_L .

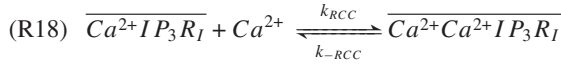
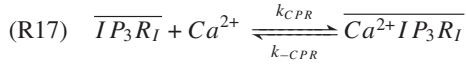
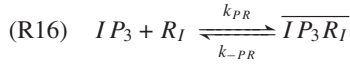
A: Desensitization of R_L by PKC.



B: Phosphorylation of PLC by PKC.



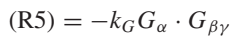
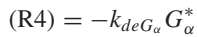
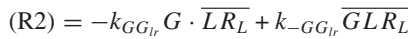
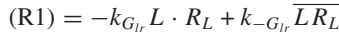
Output.



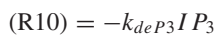
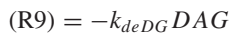
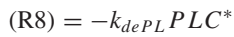
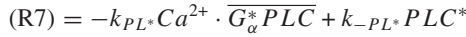
2.4. The mathematical model

The rate of Ca^{2+} release from the ER is assumed to be proportional to the product of the fraction of channels in the open state and the concentration difference between the ER and the cytosol, while the SERCA flux follows the Hill function with exponent two; all other steps are mass action. These assumptions lead to the following set of rates for individual steps, and these will then be combined to produce the governing differential equations. Notice that the previous IP_3 - Ca^{2+} model [59] was identified as the output module in modular approach.

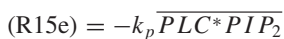
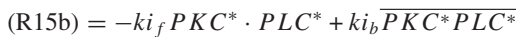
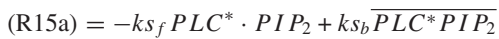
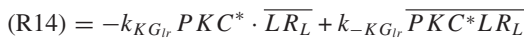
Input.



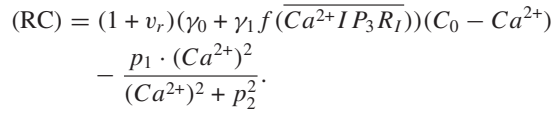
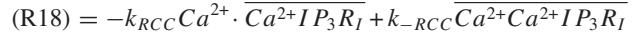
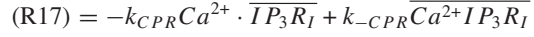
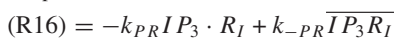
Amplification.



Feedback.



Output.



The reactions conserve a number of species, namely, PKC, mGluR, G-protein, PLC and IP_3R , which leads to the following conservation conditions:

$$PKC_0 = PKC + \overline{CaPKC} + \overline{CaPKCDAG} + \overline{PKC^* LR_L} + PKC^* + \overline{PKC^* PLC^*} + \overline{PKC^* PLC^* PIP_2} \quad (1)$$

$$R_{L0} = R_L + \overline{LR_L} + \overline{GLR_L} + \overline{PKC^* LR_L} \quad (2)$$

$$G_0 = G + G_{\beta\gamma} + \overline{GLR_L} \quad (3)$$

$$PLC_0 = PLC + \overline{G_\alpha^* PLC} + PLC^* + \overline{PKC^* PLC^*} + \overline{PKC^* PLC^* PIP_2} + \overline{PLC^* PIP_2} \quad (4)$$

$$G_{\beta\gamma} = G_\alpha GDP + G_\alpha^* + \overline{G_\alpha^* PLC} + PLC^* + \overline{PKC^* PLC^*} + \overline{PKC^* PLC^* PIP_2} + \overline{PLC^* PIP_2} \quad (5)$$

$$nR_{I0} = R_I + \overline{IP_3R_I} + \overline{Ca^{2+} IP_3R_I} + \overline{Ca^{2+} Ca^{2+} IP_3R_I} \quad (6)$$

One can easily check those relationships simply by adding the appropriate differential equations. We choose $\overline{PKC^* LR_L}$, $\overline{GLR_L}$, G , $\overline{G_\alpha^* PLC}$, G_α and $\overline{Ca^{2+} Ca^{2+} IP_3R_I}$ as dependent variables, and we solve equations (1)–(6) for these dependent variables. If we use these expressions in place of the dependent variables of (R1)–(R18) and (RC), we get a system of ordinary differential equations for the independent variables:

$$\frac{d}{dt} R_L = (R1) \quad R_L(0) = 1 \quad (7)$$

$$\frac{d}{dt} \overline{LR_L} = -(R1) + (R2) + (R14) - (R3) \quad \overline{LR_L}(0) = 0 \quad (8)$$

$$\frac{d}{dt} G_\alpha^* = -(R3) + (R4) + (R6) \quad G_\alpha^*(0) = 0 \quad (9)$$

$$\frac{d}{dt} G_{\beta\gamma} = -(R3) + (R5) \quad G_{\beta\gamma}(0) = 0 \quad (10)$$

$$\frac{d}{dt} PLC = (R6) - (R8) \quad PLC(0) = 0.8 \quad (11)$$

$$\frac{d}{dt} IP_3 = (R10) - (R15e) + (R16) \quad IP_3(0) = 0 \quad (12)$$

$$\frac{d}{dt} DAG = (R9) + (R12) - (R15e) \quad DAG(0) = 0 \quad (13)$$

$$\frac{d}{dt} PKC = (R11) \quad PKC(0) = 1.087 \quad (14)$$

$$\frac{d}{dt} \overline{Ca^{2+} PKC} = -(R11) + (R12) \quad \overline{Ca^{2+} PKC}(0) = 0.013 \quad (15)$$

$$\frac{d}{dt} \overline{Ca^{2+} DAG PKC} = -(R12) + (R13) \quad \overline{Ca^{2+} DAG PKC}(0) = 0 \quad (16)$$

$$\frac{d}{dt}R_I = (R16) \quad R_I(0) = 0.8 \quad (17)$$

$$\frac{d}{dt}\overline{IP_3R_I} = -(R16) + (R17) \quad \overline{IP_3R_I}(0) = 0 \quad (18)$$

$$\frac{d}{dt}\overline{Ca^{2+}IP_3R_I} = -(R18) \quad \overline{Ca^{2+}IP_3R_I}(0) = 0 \quad (19)$$

$$\frac{d}{dt}Ca^{2+} = (Rc) \quad Ca^{2+}(0) = 0.02 \quad (20)$$

$$\frac{d}{dt}PLC^* = -(R7) + (R8) + (R15a) + (R15b) \quad (21)$$

$$PLC^*(0) = 0$$

$$\frac{d}{dt}\overline{PLC^*PIP_2} = (R15d) + (R15e) \quad (22)$$

$$\overline{PLC^*PIP_2}(0) = 0$$

$$\frac{d}{dt}PKC^* = -(R13) + (R14) + (R15b) + (R15d) \quad (23)$$

$$PKC^*(0) = 0$$

$$\frac{d}{dt}\overline{PKC^*PLC^*} = -(R15b) + (R15c) \quad (24)$$

$$\overline{PKC^*PLC^*}(0) = 0$$

$$\frac{d}{dt}\overline{PKC^*PLC^*PIP_2} = -(R15c) - (R15d) \quad (25)$$

$$\overline{PKC^*PLC^*PIP_2}(0) = 0.$$

The initial conditions have been chosen assuming no basal stimulus or activities (table 3).

2.5. Parameters

Most of the parameter values given in table 3 were adopted from published data [20], although not all parameter values matched with specific cell types. However, some of the rate constants needed in the present study are not available in the literature or databases, and they were approximated so that the model can reproduce the experimental results from other studies. We will also use these parameters for bifurcation analysis to investigate the feedback mechanism responsible for Ca^{2+} oscillations. The units of concentrations are in μM , and the units of rate constants and equilibrium constants are described in table 3. Note that both cytosolic species and membrane-associated species have the same units (μM).

A first step in understanding the system might be to identify scalings for the variables and to define dimensionless parameters, but we will defer this to another paper in which spatial effects are included, since the multiple time and space scales are intimately linked. The biochemical step (R15a)–(R15e) are left as mass action kinetic equations by the same token, although they are easily converted into a form of the Hill-type function by different time scale arguments.

Here we will explore the full model computationally with the objective of understanding how the processes interact to influence the dynamics. As was discussed earlier, there are a number of interacting feedback loops that can either be positive or negative, depending on the state of the system,

and thus one can anticipate that a detailed parametric study of the dynamics might reveal regimes in parameter space in which the dynamics are qualitatively different. The binding rate of PKC and R_L (k_{PKLR}), as well as the rate constants related to the inhibitory action of PKC on PLC are unknown, and they were determined by comparing numerical solutions with published data. The production rate of IP_3 and DAG by activated PLC (k_p) is also unknown, and has been chosen as a parameter for the bifurcation analysis. Finally, two different values of the inactivation rate of active PKC (k_{-PK^*}) have been chosen to simulate different cell types.

3. Results and discussion

3.1. Bifurcation analysis: four modes of Ca^{2+} responses for variable PKC and PLC activities

As was stated earlier, the two major types of Ca^{2+} oscillations under sustained agonist stimulus are BLS and SO, and PKC is thought to be an important factor in controlling the transition between them by modulating the intracellular $[IP_3]$ level [14, 57, 67]. Many different factors affect IP_3 levels, including the activities of PKC and PLC and the glutamate concentration. We first consider the effects of PKC and PLC activities and later study the effect of changes in the stimulus level (the glutamate concentration). We use k_{PK^*} as a measure of the PKC activity, and k_p as a measure of PLC activity. The former controls the membrane binding rate that is the last stage of PKC activation, and the latter governs the rate of PIP_2 hydrolysis, hence of IP_3 production. Thus these parameters can be viewed as measures of the strength of the feedback, and of the signal amplification, respectively (figure 2). In the first step, the steady-state levels of all variables, which are obtained by setting the right-hand sides of equations (7)–(25) to zero and solving the resulting algebraic system, were computed as a function of k_p for various levels of PKC activity, and the results are shown in figure 3. Beginning at low k_p , the steady-state level of Ca^{2+} is expected to increase as k_p is increased if the increase in PLC^* activity, and the increased hydrolysis rate of PIP_2 and elevation in $[IP_3]$ that result, offset the feedback effect of Ca^{2+} -dependent activation of PKC^* (figures 3(A)–(C)). Nonetheless, the increased level of PKC^* blocks PLC activation by GPCR inhibition (figure 2), and the steady-state level of activated PLC, $[PLC^*]_{ss}$, will decrease as k_p increases. Figure 3(D) confirms this, except when there is no PKC feedback, i.e., when $k_{PK^*} = 0$, or $[PKC^*]_{ss} = 0$. Although $[PLC^*]_{ss}$ decreases as k_p increases, the steady-state level of $[IP_3]$ ($[IP_3]_{ss}$) rises steadily (figure 3(B)), which indicates that the more rapid formation of IP_3 via reaction R15e more than offsets the inhibitory effect of increased PKC^* . Despite the fact that the total concentration of PKC and PLC are $0.8 \mu M$ and $1.1 \mu M$ respectively, their activated levels, PKC^* and PLC^* , remain in the nanomolar range (figures 3(C) and (D)).

The changes in the steady-state levels of $[Ca^{2+}]$ ($[Ca^{2+}]_{ss}$) and $[IP_3]$ in response to changes in k_p and k_{PK^*} sheds light on the interaction of PLC^* and PKC^* . When $k_{PK^*} = 0$, $[PKC^*]_{ss} = 0$ and $[IP_3]_{ss}$ increases linearly with k_p , while

Table 3. Parameters and their values and meaning.

Parameter	Meaning	Value	Unit	Source
k_{on}	On rate for L and R_L	16.8	$(\mu\text{M} \cdot \text{s})^{-1}$	[20, 58, 7, 54, 27, 61, 5, 34, 52]
k_{off}	Off rate for L and R_L	10	$(\text{s})^{-1}$	[20, 58, 7, 54, 27, 61, 5, 34, 52]
k_{GGI_r}	On rate for $L \cdot R_L$ and G -protein	0.006	$(\mu\text{M} \cdot \text{s})^{-1}$	[20, 58, 7, 54, 27, 61, 5, 34, 52]
k_{-GGI_r}	Maximal kinetic off rate for $L \cdot R_L$ and G -protein	0.0001	$(\text{s})^{-1}$	[20, 58, 7, 54, 27, 61, 5, 34, 52]
k_{G_α}	GTP and GDP switching rate on $G \cdot L \cdot R_L$ complex	0.01	$(\mu\text{M} \cdot \text{s})^{-1}$	[20, 58, 7, 54, 27, 61, 5, 34, 52]
k_{deG_α}	G_α^* ($= G_\alpha \cdot GTP$) hydrolysis rate	0.0133	$(\text{s})^{-1}$	[20, 58, 7, 54, 27, 61, 5, 34, 52]
k_G	On rate for G_α and $G_{\beta\gamma}$	6	$(\mu\text{M} \cdot \text{s})^{-1}$	[20, 58, 7, 54, 27, 61, 5, 34, 52]
k_{GPL}	On rate of PLC by G_α^* ($= G_\alpha \cdot GTP$)	2.25	$(\mu\text{M} \cdot \text{s})^{-1}$	[20, 58, 7, 54, 27, 61, 5, 34, 52]
k_{-GPL}	Off rate of PLC against G_α^* ($= G_\alpha \cdot GTP$)	1	$(\text{s})^{-1}$	[20, 58, 7, 54, 27, 61, 5, 34, 52]
k_{PL^*}	Activation rate of $G_\alpha^* \cdot PLC$ by Ca^{2+}	30	$(\mu\text{M} \cdot \text{s})^{-1}$	[20, 58, 7, 54, 27, 61, 5, 34, 52]
k_{-PL^*}	Deactivation rate of PLC^* into $G_\alpha^* \cdot PLC$ by Ca^{2+}	1	$(\text{s})^{-1}$	[20, 58, 7, 54, 27, 61, 5, 34, 52]
k_{dePL}	Degradation rate of PLC^*	1.667	$(\text{s})^{-1}$	[20, 58, 7, 54, 27, 61, 5, 34, 52]
k_{deDG}	Rate constant of DAG degradation	0.15	$(\text{s})^{-1}$	[20, 58, 7, 54, 27, 61, 5, 34, 52]
k_{deP3}	Rate constant of IP_3 degradation	2.5	$(\text{s})^{-1}$	[20, 58, 7, 54, 27, 61, 5, 34, 52]
k_{CK}	On rate for Ca^{2+} and PKC	0.6	$(\mu\text{M} \cdot \text{s})^{-1}$	[20, 58, 7, 54, 27, 61, 5, 34, 52]
k_{-CK}	Off rate for and Ca^{2+} and PKC	0.5	$(\text{s})^{-1}$	[20, 58, 7, 54, 27, 61, 5, 34, 52]
k_{CKDG}	On rate for $Ca^{2+} \cdot PKC$ and DAG	0.007998	$(\mu\text{M} \cdot \text{s})^{-1}$	[20, 58, 7, 54, 27, 61, 5, 34, 52]
k_{-CKDG}	Off rate for $Ca^{2+} \cdot PKC \cdot DAG$	8.6348	$(\text{s})^{-1}$	[20, 58, 7, 54, 27, 61, 5, 34, 52]
k_{PK^*}	Activation rate of $Ca^{2+} \cdot PKC \cdot DAG$	1	$(\mu\text{M} \cdot \text{s})^{-1}$	[20]/Bifurcation parameter
k_{-PK^*}	Inactivation rate for $PKC^*=(Ca^{2+} \cdot PKC \cdot DAG)^*$	0.1, (60)	$(\text{s})^{-1}$	[20]/Cell type specific
k_{PKLR}	R_L phosphorylation rate by PKC	(25)	$(\mu\text{M} \cdot \text{s})^{-1}$	
k_{-PKLR}	R_L dephosphorylation rate	(0.1)	$(\text{s})^{-1}$	
k_p	Hydrolysis rate of PIP_2 by PLC^*	100 (0 ~ 350)	$(\text{s})^{-1}$	Bifurcation parameter
ks_f	On rate for PIP_2 and $PLC^*/PKC^* \cdot PLC^*$	1e3	$(\mu\text{M} \cdot \text{s})^{-1}$	
ks_b	Off rate for PIP_2 and $PLC^*/PKC^* \cdot PLC^*$	1e3	$(\text{s})^{-1}$	
ki_f	On rate for PKC^* and $PLC^*/PLC^* \cdot PIP_2$	1e8	$(\mu\text{M} \cdot \text{s})^{-1}$	
ki_b	Off rate for PKC^* and $PLC^*/PLC^* \cdot PIP_2$	5e3	$(\text{s})^{-1}$	
R_{L0}	Free glutamate receptor concentration	1	μM	[20, 58, 7, 54, 27, 61, 5, 34, 52]
G_0	Total G -protein concentration	1	μM	[20, 58, 7, 54, 27, 61, 5, 34, 52]
PLC_0	Total PLC concentration	0.8	μM	[20, 58, 7, 54, 27, 61, 5, 34, 52]
PIP_2	Total PIP_2 and its derivatives concentration	25	μM	[20, 58, 7, 54, 27, 61, 5, 34, 52]
PKC_0	Total PKC concentration	1.1	μM	[20, 58, 7, 54, 27, 61, 5, 34, 52]
R_{I0}	Total IP_3 receptor concentration	0.8	μM	[20, 58, 7, 54, 27, 61, 5, 34, 52]
GTP	GTP concentration in the cell	10	μM	[20, 58, 7, 54, 27, 61, 5, 34, 52]
L	Glutamate concentration	1 ~ 100	μM	[13]
k_{PR}	IP_3 binding rate to R_I	12	$(\mu\text{M} \cdot \text{s})^{-1}$	[59, 20]
k_{-PR}	Kinetic off rate for $IP_3 \cdot R_I$	8	$(\text{s})^{-1}$	[59, 20]
k_{CPR}	Kinetic on rate for Ca^{2+} and $IP_3 \cdot R_I$	15	$(\mu\text{M} \cdot \text{s})^{-1}$	[59, 20]
k_{-CPR}	Kinetic off rate for $Ca^{2+} \cdot IP_3 \cdot R_I$	1.65	$(\text{s})^{-1}$	[59, 20]
k_{RCC}	Kinetic on rate for Ca^{2+} and $Ca^{2+} \cdot IP_3 \cdot R_I$	1.8	$(\mu\text{M} \cdot \text{s})^{-1}$	[59, 20]
k_{-RCC}	Kinetic off rate for $Ca^{2+} \cdot Ca^{2+} \cdot IP_3 \cdot R_I$	0.21	$(\text{s})^{-1}$	[59, 20]
v_r	ER /cytosol volume ratio	0.85	unitless	[59, 20]
γ_0	Basal Ca^{2+} permeability of the ER	0.1	$(\text{s})^{-1}$	[59, 20]
γ_1	Sensitivity of IP_3 -gated channels on the ER to IP_3	20	$(\text{s})^{-1}$	[59, 20]
p_1	The Ca^{2+} pumping parameter	(6)	unitless	modified from [59, 20]
p_2	The Ca^{2+} pumping parameter	(0.45)	unitless	modified from [59, 20]
C_0	The average Ca^{2+} concentration in a cell	1.56 μM	μM	[59, 20]

nonzero $[PKC^*]_{ss}$ retards the rate of increase in $[IP_3]_{ss}$ (figure 3(B)). $[Ca_i^{2+}]_{ss}$ shows a pattern similar to $[IP_3]_{ss}$, namely, it is an increasing function of k_p and a decreasing function of k_{PK^*} . Note that when $k_{PK^*} = 0$ the system is similar to the CICR–SERCA model [59] except for the additional amplifying mechanism via PLC^* . It was shown that the CICR–SERCA model can be understood as an excitable system and Ca_i^{2+} oscillations can be found for a suitable interval of $[IP_3]$ [83]. Here the balance between the effects of k_p and k_{PK^*} can also destabilize the steady state, and as shown in figure 3, periodic oscillations exist in an

intermediate range of k_p . Because k_{PK^*} directly affects the level of $[PKC^*]_{ss}$, $[PKC^*]_{ss}$ increases as k_{PK^*} increases, while $[PLC^*]_{ss}$ decreases due to the PKC^* feedback on the input module (figures 3(C) and (D)). In figures 3(C) and (D), we see that periodic solutions exist at intermediate levels of $[PLC^*]_{ss}$ and $[PKC^*]_{ss}$, and that excessive levels of either $[PLC^*]_{ss}$ or $[PKC^*]_{ss}$ abolish the periodic solution.

In our two-parameter analysis, the balance between the PLC and PKC activities controls the steady-state levels of all components, but it also determines the nature of the transitions between Ca_i^{2+} response patterns. For $0.2 \lesssim$

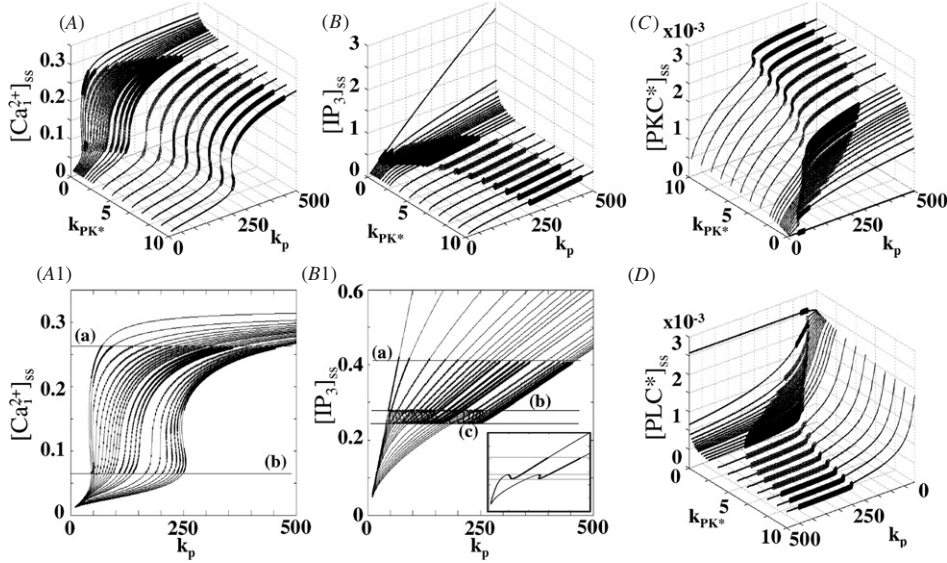


Figure 3. Parametric dependence of the steady state solutions. Shown are $[\text{Ca}_i^{2+}]_{ss}$ (A), $[\text{IP}_3]_{ss}$ (B), and $[\text{PKC}^*]_{ss}$ (C) in μM as functions of k_p and k_{PK^*} vary. The projections of (A) and (B) onto the respective k_p planes are shown in (A1) and (B1), where in (A1) lines (a) and (b) represent $[\text{Ca}_i^{2+}]_{ss} = 0.26$ and 0.064 (μM) respectively, and in (B1) lines (a), (b) and (c) represent $[\text{IP}_3]_{ss} = 0.42$, 0 , 0.278 and 0.247 (μM) respectively. Inset shows $[\text{IP}_3]_{ss}(k_p)$ at $k_{PK^*} = 1$ and 10 respectively. (C) Steady-state levels of $[\text{PKC}^*]_{ss}$ and of PLC^* (D), as functions of k_p and k_{PK^*} . Parameter regions in which periodic solutions are denoted by thickened lines. Steady state of Ca_i^{2+} , $[\text{IP}_3]$, PLC^* are low for small k_p and k_{PK^*} and high for large k_p and k_{PK^*} , while $[\text{PLC}^*]_{ss}$ varies inversely (note that k_p is plotted in descending order for clarity in (D)). At high k_p , although $[\text{PLC}^*]_{ss}$ takes lower value because of stronger GPCR inhibition by high $[\text{PKC}^*]_{ss}$, escalation in $[\text{IP}_3]_{ss}$ indicates that stronger PLC activity at higher k_p .

$k_{PK^*} \lesssim 8$, $[\text{IP}_3]_{ss}$ increases with k_p , and when it reaches a certain level (figure 3(B1)-(b), $[\text{IP}_3]_{ss} \simeq 0.278$), a periodic solution bifurcates from the steady state. A further increase in k_p leads to a decrease in $[\text{IP}_3]_{ss}$ (figure 3(B1)-(b)→(c)) in which the time-averaged oscillatory IP_3 level ($\lim_{T \rightarrow \infty} \frac{1}{T} \int_0^T \text{IP}_3(k_p, k_{PK^*}) dt$) is kept constant approximately at 0.28 for $93.7 \lesssim k_p \lesssim 117.75$ (the inset of figure 4(B)). Beyond this interval, which terminates at the turning point (figure 3(B1)-(c) $[\text{IP}_3]_{ss} \simeq 0.247$), $[\text{IP}_3]_{ss}$ increases as k_p increases until the system regains stability (figure 3(B1)-(a): $[\text{IP}_3]_{ss} \simeq 0.42$). For $k_{PK^*} \gtrsim 8$ and $k_{PK^*} \lesssim 0.2$, the system has multiple steady-state solutions (figures 3(A1) and (B1)).

The shape of the steady-state curve for $[\text{Ca}_i^{2+}]_{ss}$, and in particular the existence of multiple steady states, is inherited from the CICR–SERCA model, and for $0.2 \lesssim k_{PK^*} \lesssim 8$, $[\text{Ca}_i^{2+}]_{ss}$ is a monotone increasing function of k_p . The steady-state level of $[\text{Ca}_i^{2+}]_{ss}$ when the steady state loses stability is $[\text{Ca}_i^{2+}]_{ss} \simeq 0.064$, (figure 3(A1)-(b)) and when stability is recovered $[\text{Ca}_i^{2+}]_{ss} \simeq 0.26$ (figure 3(A1)-(a)). The oscillations near the first bifurcation point are of BLS type, whereas when they disappear at large k_p they are of TP type. We find numerically that the $[\text{IP}_3]_{ss}$ and $[\text{Ca}_i^{2+}]_{ss}$ levels at the lower (BLS) and upper (TP) bifurcation points are essentially independent of k_p and k_{PK^*} , which means that the Ca_i^{2+} and $[\text{IP}_3]$ levels can be regarded as characteristic kinetic values associated with the output module, independent of the other modules.

Next, the bifurcating periodic solutions are plotted as either a function of PLC activity (k_p) with PKC activity fixed

($k_{PK^*} = 1$), (i.e., along the $\overline{\text{H1H2}}$ in figure 4(A)) or as a function of PKC activity (k_{PK^*}) with PLC activity fixed ($k_p = 200$), (i.e., along the $\overline{\text{H3H4}}$ in figure 4(A)). Figure 4(C) shows that the steady-state $[\text{Ca}_i^{2+}]$ level increases as k_p increases, and the steady state loses stability via a subcritical Hopf bifurcation at H1, where a periodic solution emerges (figures 4(A) and (C)). For large k_p , the steady state recovers its stability via a supercritical Hopf bifurcation (H2), and the stable steady has elevated $[\text{Ca}_i^{2+}]$. The frequency of $[\text{Ca}_i^{2+}]$ oscillations increases monotonically (figure 4(D)) and the amplitudes of the peaks of oscillation decrease as k_p increases (figure 4(C)). The steady-state level of $[\text{IP}_3]$ is also an increasing function of k_p except for the region near H1, where the BLS-type $[\text{Ca}_i^{2+}]$ response occurs. The amplitudes of the IP_3 oscillations are small compared with those of Ca^{2+} , and the maximum and minimum increase monotonically in the SO regime. By comparing figure 4(B) with (E), (C) with (F) and (D) with (G), one sees that similar response diagrams in $[\text{Ca}_i^{2+}]$ and $[\text{IP}_3]$ are obtained by decreasing k_{PK^*} at fixed k_p along $\overline{\text{H4H3}}$ in figure 4(A).

Thus both baseline $[\text{Ca}_i^{2+}]$ and $[\text{IP}_3]$ increase with increasing PLC activity except near the boundary of the oscillatory regime ($\overline{\text{H1H4}}$ in figure 4(A)). When the steady-state level of $[\text{IP}_3]$ is high enough to open a significant fraction of calcium channels, both $[\text{IP}_3]$ and $[\text{Ca}_i^{2+}]$ begin to oscillate. Near the onset of oscillations ($\overline{\text{H1H4}}$), the dynamics can be characterized as low frequency, constant amplitude $[\text{Ca}_i^{2+}]$ oscillations, as shown in the circled region in figure 4(C), and a comparatively low $[\text{IP}_3]$, which defines the BLS regime.

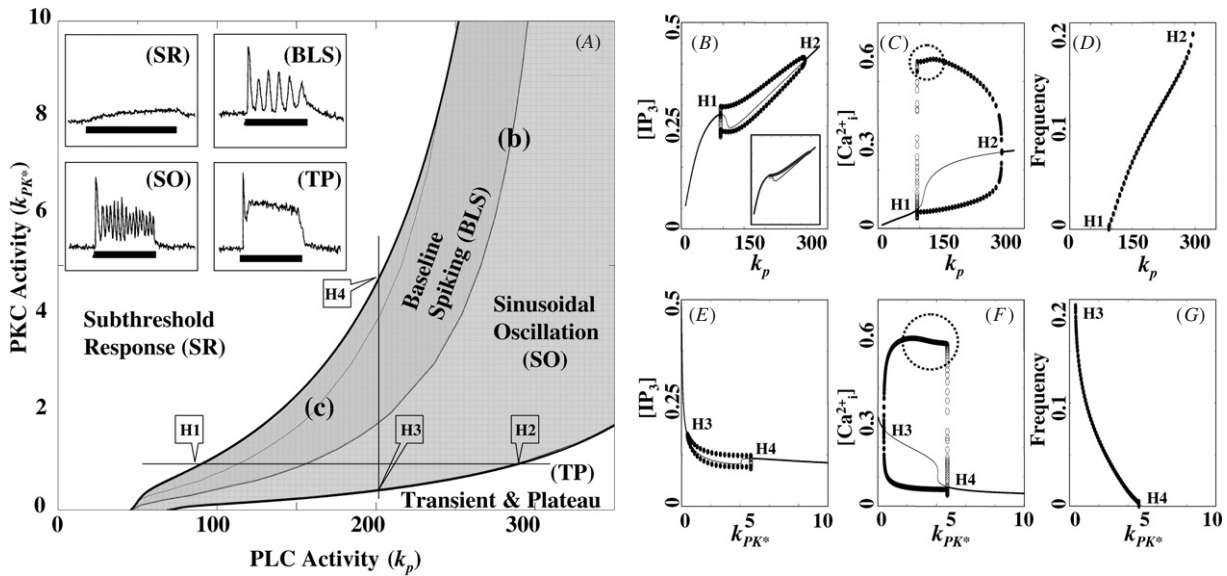


Figure 4. Bifurcation diagrams and examples of typical $[Ca_i^{2+}]$ response patterns computed for the model. (A) For small k_p the $[Ca_i^{2+}]$ response in response to small perturbations is a small subthreshold response (SR). The curves (c) and (b) represent the turning points and the second intersection of the plane $[IP_3]_{ss} = 0.278$ with the $[IP_3]_{ss}$ manifold as in figure 3(B1). At the point H1, where a periodic solution bifurcates from the steady state, the $[Ca_i^{2+}]$ response is a low-frequency oscillation initiated from the baseline (baseline spiking: BLS). For higher k_p (larger than (b)), sustained high-frequency $[Ca_i^{2+}]$ oscillations are observed (sinusoidal oscillation: SO). For k_p greater than the value at H2 the steady state is again locally stable, no sustained oscillations are observed, and $[Ca_i^{2+}]$ approaches an elevated steady-state value after an initial transient spike (transient and plateau: TP). Insets show various Ca_i^{2+} responses observed in astrocytes either under physiological or abnormal conditions [43]. Solid bars in the insets denote periods of stimulation. (B)–(D): solution structure of $[IP_3]$ (B), $[Ca_i^{2+}]$ (C) as k_p varies along $\overline{H1H2}$ and frequency of $[Ca_i^{2+}]$ oscillation between H1 and H2 (D). The inset in (B) shows the averaged value of $[IP_3]$ computed by evaluating $\frac{1}{T} \int_0^T IP_3(k_p, k_{PK^*}) dt$ for some large T (3000). (E)–(G): solution structure of $[IP_3]$ (E), $[Ca_i^{2+}]$ (F) as k_{PK^*} varies along $\overline{H3H4}$ and the frequency of $[Ca_i^{2+}]$ oscillations between H3 and H4 (G). In (B), (C), (E) and (F), solid lines denote the steady state, and filled (empty) circles denote the maximal and minimal amplitude of the component along a stable (filled) or unstable (empty) periodic solution. (B) and (E) show that the range of $[IP_3]$ remains constant near the first bifurcation point. (C) and (F) show that near the first bifurcation point, the amplitude of Ca_i^{2+} spikes is approximately constant, which is a characteristic property of BLS, while there is a significant amplitude change at high k_p and k_{PK^*} , which is a major property of SO. The frequency profiles in (D) and (G) also have two distinct regions. Near the first bifurcation point the frequency changes rapidly from zero, and then the rate of frequency change decreases. At high $[IP_3]$.

Tomas *et al* [88] pointed out that an important characteristic of the BLS regime is that the amplitude of the $[Ca_i^{2+}]$ oscillations is independent of the stimulus level (table 1).

At higher $[IP_3]$ production rates the $[Ca_i^{2+}]$ trace shows an elevated high $[Ca_i^{2+}]$ steady state, and lower amplitude, high-frequency oscillations, which are the characteristics of SO (figures 4(A), (C) and (D)). At even higher k_p (and hence $[IP_3]$), the calcium response saturates and the steady state recovers its stability. In this regime $[Ca_i^{2+}]$ responses are damped oscillations that converge to an elevated steady state of $[Ca_i^{2+}]$, or alternatively, there is an initial $[Ca_i^{2+}]$ transient followed by a plateau (TP).

By continuing the two Hopf points H1 and H2 in figure 4(A) in the two parameters k_p and k_{PK^*} , the boundary of the oscillatory domain in the $k_{PK^*} \times k_p$ plane can be determined. In the region between the first bifurcation point (H1H4) and the turning points in the steady-state diagram (figure 4(A)-(c)), $[IP_3]_{ss}$ decreases, and the BLS-type oscillations exist in this region.

Qualitatively the $[Ca_i^{2+}]$ response undergoes similar transitions at each fixed PKC activity (as measured by k_{PK^*}),

although the intervals of periodic activity vary (cf figure 4). Increasing the PKC activity widens the range of k_p in which the components oscillate, and the value of k_{PK^*} at which oscillations set in increases monotonically with k_p . Even at zero PKC activity, oscillatory $[Ca_i^{2+}]$ oscillations are observed for a small range of PLC activities. The two-parameter bifurcation diagram divides the parameter space into ‘equivalence’ classes within which the solutions are qualitatively similar. This allows us to classify all the possible $[Ca_i^{2+}]$ response patterns under sustained agonist stimulus in $k_p \times k_{PK^*}$ space into the following four equivalence classes: SR, BLS, SO and TP (figure 4(A)). This classification corresponds with the experimentally-observed $[Ca_i^{2+}]$ responses in astrocytes [43] (cf insets in figure 4(A)).

One can anticipate that the computed two-parameter bifurcation diagram of PLC activity versus PKC activity is similar to that of glutamate concentration versus PKC activity, since the glutamate input level is transduced into PLC, which produces IP_3 , which in turn mobilizes the luminal Ca^{2+} . This is borne out by a comparison of the glutamate concentration versus PKC activity diagram shown in figure 7(D) with that shown in figure 4(A).

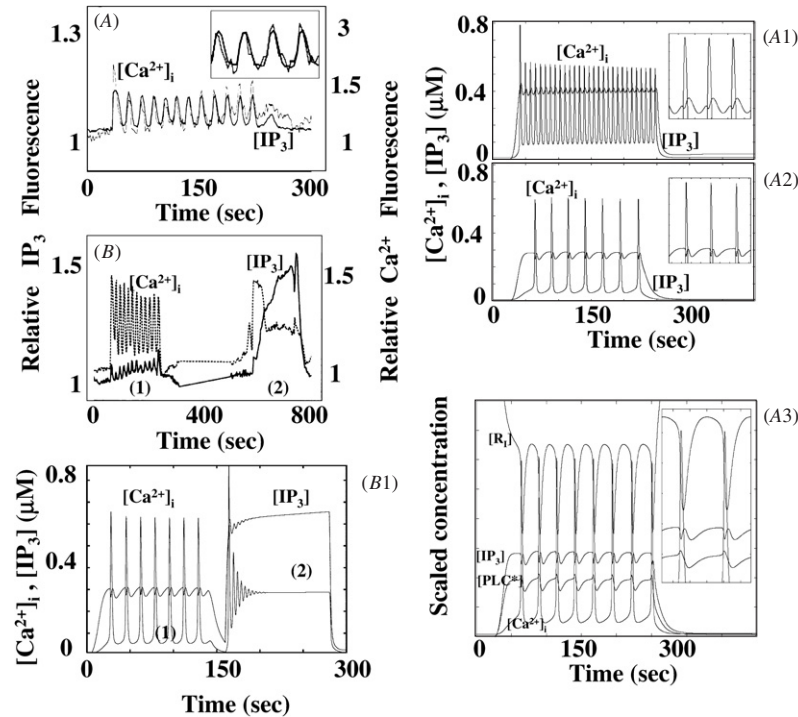


Figure 5. Experimental data from ([57]) versus the theoretical predictions. (A) and (B) are adopted from [56, 57] and the others are from the simulation. (A): In mGluR-expressing cells, the peaks of $[\text{IP}_3]$ and $[\text{Ca}_i^{2+}]$ are highly coincident, when 1 mM glutamate is applied. (A1) and (A2): the simultaneous oscillation of $[\text{Ca}_i^{2+}]$ and $[\text{IP}_3]$ when $k_{PK^*} = 1$ (the condition for a wild-type cell) with different levels of $[\text{IP}_3]$. For higher $[\text{IP}_3]$ ($k_p = 150$), the $[\text{IP}_3]$ oscillation synchronizes with the $[\text{Ca}_i^{2+}]$ oscillation (A1). However, for BLS ($k_p = 70$), $[\text{IP}_3]$ suddenly decrease at the moment $[\text{Ca}_i^{2+}]$ peaks occur (A2). (A3): the traces of $[\text{Ca}_i^{2+}]$, $[\text{IP}_3]$, PLC^* and R_f (free IP_3 receptors) at BLS. The traces of PLC^* and R_f indicate that the sudden decrease of $[\text{IP}_3]$ comes from R_f binding rather than PLC^* inhibition (See the text). Insets of (A1), (A2) and (A3) show a magnified view of a few spikes. (B): The cells showed $[\text{IP}_3]$ and $[\text{Ca}_i^{2+}]$ oscillations, when glutamate ($100 \mu\text{M}$) is applied (1), while $[\text{IP}_3]$ increased and $[\text{IP}_3]$ and $[\text{Ca}_i^{2+}]$ oscillations disappear even at the same level of glutamate stimulation when the cells were treated by PKC inhibitor ($1 \mu\text{M}$ staurosporine: 2). (B1): At $k_{PK^*} = 1$ and $k_p = 100$ (condition for a wild-type cell), the model shows $[\text{IP}_3]$ and $[\text{Ca}_i^{2+}]$ oscillation (1). When PKC activity was lowered ($k_{PK^*} = 0$, $k_p = 100$), $[\text{IP}_3]$ and $[\text{Ca}_i^{2+}]$ oscillations disappeared similar to (B).

3.2. Oscillations of IP_3 with $[\text{Ca}_i^{2+}]$

To test the validity of the model and the conclusions drawn from the bifurcation analysis, the temporal dynamics of each species were compared with experimental data. Recall that whether or not $[\text{IP}_3]$ oscillates with $[\text{Ca}_i^{2+}]$ is important for determining the underlying mechanism of $[\text{Ca}_i^{2+}]$ oscillation. In the study by Nash *et al* [57], $[\text{IP}_3]$ and $[\text{Ca}_i^{2+}]$ oscillate in synchrony in mGluR-expressing cells at normal PKC activity levels (cf figures 5(A) and (B)-(1), $t = 0-250$ s). When the PKC activity is blocked, the increased $[\text{IP}_3]$ level is sustained and no $[\text{IP}_3]$ oscillation is observed (figure 5(B)-(2), $t > 600$ s). A comparison with the model predictions shows excellent agreement (cf figures 5(B1)-(1) and (2)).

The model predicts that $[\text{IP}_3]$ and $[\text{Ca}_i^{2+}]$ oscillations exhibit coincident timings of their minima and maxima in the SO regime, but in the BLS regime $[\text{IP}_3]$ drops just before the peak of $[\text{Ca}_i^{2+}]$ occurs (figures 5-(A1) and (A2)). This can be explained by the fact that a large portion of IP_3 is bound to R_f in the BLS regime, when $[\text{IP}_3]$ is low, while a smaller fraction of IP_3 participates in IP_3 -gated Ca^{2+} channel opening at high $[\text{IP}_3]$. Figure 5(A3) also supports this argument. If

the sudden drop of $[\text{IP}_3]$ were due to the inhibitory action of PKC^* on PLC^* , a sudden decrease of PLC^* would precede this. However, the minima and maxima of $[\text{Ca}_i^{2+}]$ and PLC^* spikes are highly coincident and antiphase to the R_f spikes, which implies that IP_3 decreases due to binding to R_f rather than that IP_3 production has been inhibited. For this reason, it may be difficult to record $[\text{IP}_3]$ oscillations at low $[\text{IP}_3]$ (in the BLS-type regime of $[\text{Ca}_i^{2+}]$ oscillation) (figure 5-(A2)). It is worthwhile mentioning that a recent study [97, 23] suggested that $[\text{IP}_3]$ oscillations reported experimentally could in fact be an artifact due to the experimental method (translocation of GFP-PHplc). Recall that no $[\text{IP}_3]$ oscillation is incorporated in the first type of $[\text{Ca}_i^{2+}]$ dynamics model, in which CICR and SERCA comprise the feedback loop, and regenerative CICR leads to BLS (table 1).

Figure 4 implies that SO may be the major type of oscillatory Ca_i^{2+} responses in cells, because the range of PLC activity that produces SO is much larger than that for BLS. However, it has been reported that both baseline spiking and sinusoidal oscillation can be observed in many types of cells [43], and in some cell types BLS is the only type of oscillatory Ca_i^{2+} response [100]. For the latter type, it is thought that

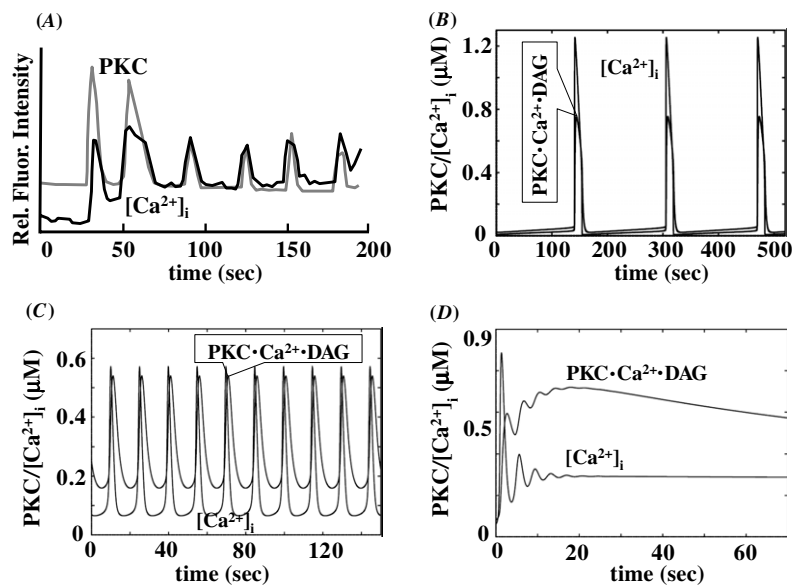


Figure 6. Oscillations of $[Ca^{2+}]_i$ and PKC. (A) figure was redrawn from [14]. Codazzi *et al* concluded that $[Ca^{2+}]_i$ and PKC oscillations are synchronized with BLS-type Ca^{2+} oscillations. (B) Model shows synchronized oscillations of $[Ca^{2+}]_i$ and PKC for BLS. In (B), $(k_{sf}, k_{sb}, k_{if}, k_{ib}) = (1e3, 5e3, 1e8, 1e3)$ were used to generate the figure and scaled PKC concentration ($\times 300$) is shown. (C) The model also predicts that each peak of the PKC spikes occurs when $[Ca^{2+}]_i$ is lowest between spikes for SO-type Ca^{2+} oscillations. (D) Beyond a certain level of PKC, $[Ca^{2+}]_i$ oscillations cease. In (C) and (D), scaled PKC concentration ($\times 1e3$) was used to compare PKC and $[Ca^{2+}]_i$ profiles with $k_p = 100, 300$ for $k_{-PK^*} = 60$.

there are additional control mechanisms that keep $[IP_3]$ levels low, because BLS can be observed only at limited levels of $[IP_3]$ (figures 4(B) and (C)) [100]. Alternatively, the kinetic properties of the 3R-gated channels may be different in those classes of cell types (figure 9).

3.3. Phase relations of the $[Ca^{2+}]_i$ and PKC oscillations

In some models of Ca^{2+} dynamics [2, 33, 36, 70, 91], PKC plays a important role in Ca^{2+} oscillations by downregulating both GPCRs and PLC. In view of the inhibitory effect of PKC on Ca^{2+} release, it could be conjectured that the Ca^{2+} and PKC profiles would not be synchronized. Some studies [17, 94] reported that $[Ca^{2+}]_i$ and PKC oscillations are out of phase, while others suggested that PKC and Ca^{2+} are synchronized [14, 75]. Our model displays both types of behavior, the former under conditions that lead to SO-type oscillations (figure 6(B)), and the latter for BLS-type oscillations (figures 6(C) and (D)). In addition, the model predicts that at high-PKC activity, the phase difference between PKC and Ca^{2+} is even more pronounced, and the oscillation of $[Ca^{2+}]_i$ can be blocked by the elevated level of PKC (figure 6(D)), while the level of PKC is maintained at a certain level in oscillatory $[Ca^{2+}]_i$ response (figures 6(A) and (B)).

If we were to assume that SO are generated by repetitive inhibition of IP_3 production by PKC, and BLS is generated by a PKC-independent CICR mechanism (table 1), we could expect that SO is the dominant type of Ca^{2+} oscillation at higher PKC activity, and that the transition from BLS to SO occurs as the strength of PKC activity increases. Young *et al* [101] observed various $[Ca^{2+}]_i$ response patterns by varying the strength of

PKC activity, but according to their study, the transition from SO (figure 7(Ab)) to BLS is observed when a cell is treated with a PKC activator (cf figure 7(Aa)). In addition, the data show that $[Ca^{2+}]_i$ oscillations disappear when PKC activity is lowered by a PKC inhibitor treatment (figure 7(Ac)), which is observed at high PKC level in figure 6(C). Significantly, the model shows the same $[Ca^{2+}]_i$ response patterns as the PKC activity level changes (figures 7(A1)–(A3)). This observation can be understood by reference to the bifurcation curves in the PKC and PLC planes under normal conditions under which the system is located in an oscillatory region, specifically in the SO region (figures 7(B)–(SO) and 7(A2)). With PLC activity fixed, the system moves up along the vertical line in figure 7(B) as the PKC activity becomes stronger, and finally enters the baseline spiking region (figures 4(B), 7(B)–(BLS)). On the other hand, as the PKC activity is inhibited, the system moves down along the vertical line where PLC activity is constant, leaves the oscillatory region and enters the transient with plateau region (figures 7(B)–(TP) and (A3)). This observation indicates that the conventional viewpoint, which distinguishes SO and BLS by PKC dependence could be problematic; it is necessary to consider the strength of PKC and PLC activity together as factors which determine SO and BLS.

Another interesting observation regarding PKC and $[Ca^{2+}]_i$ oscillations is from Nash *et al* [57]. They reported that cells treated by PKC inhibitor (PDBu) lost the periodic behavior which was usually observed before the PDBu treatment. Interestingly enough, the PKC inhibitor treated cell recovers its periodic behavior when they decrease the concentration of glutamate, the agonist used for stimulus (figure 7(C)–(Nash)). To understand this,

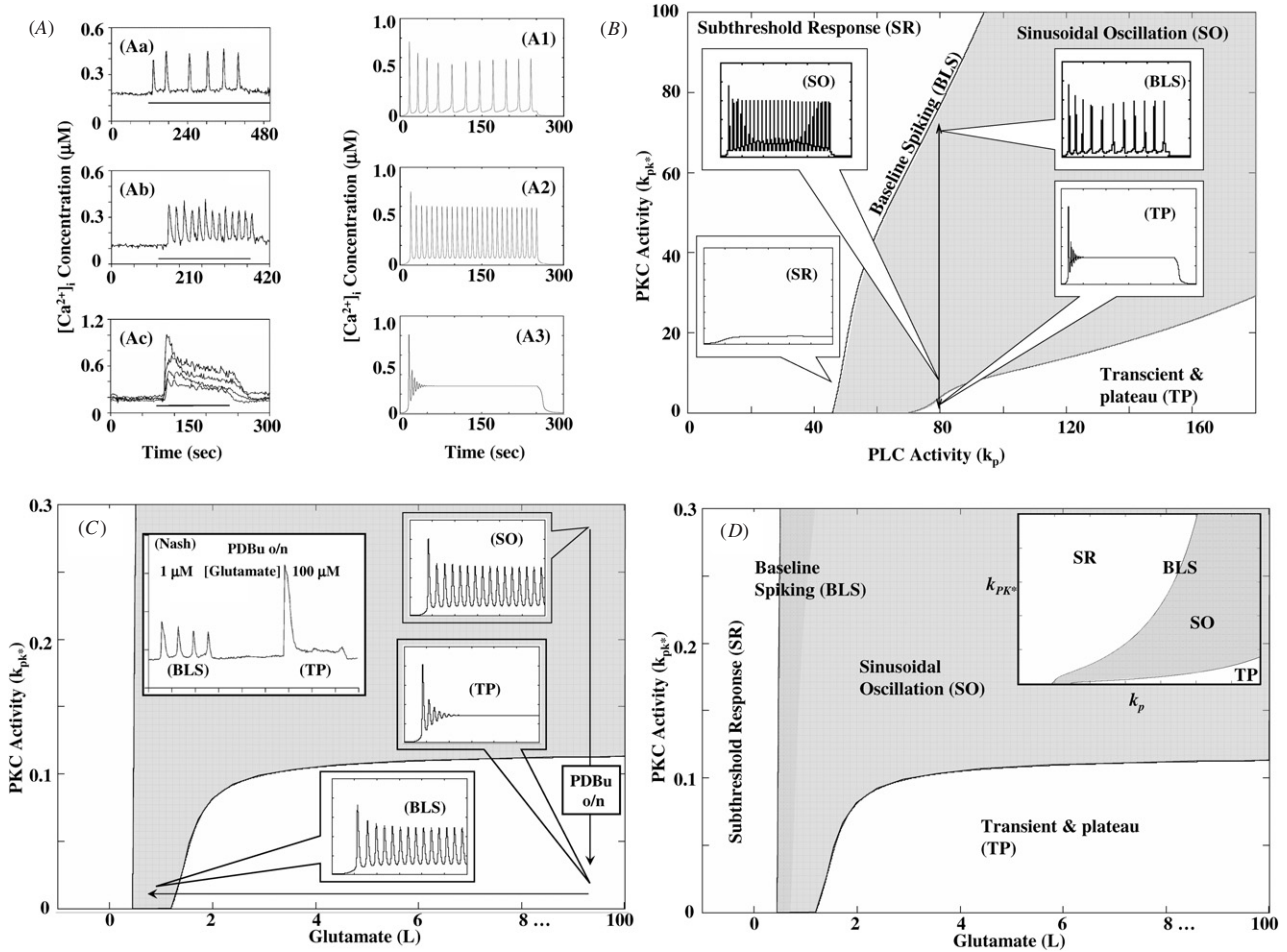


Figure 7. Experimental data versus the theoretical predictions. (A) and (B) Experimental results from [100] (Aa)–(Ac); extracellular Ca^{2+} -induced $[\text{Ca}_i^{2+}]$ oscillations without/with PKC activator, PKC inhibitor) are compared with numerical results of the model system (A1)–(A3). Under control conditions, the cell shows SO (Ab). However, when a cell is treated with a PKC inhibitor, $[\text{Ca}_i^{2+}]$ oscillations change to TP-type response (Ac). On the other hand, when a cell is treated with a PKC activator, $[\text{Ca}_i^{2+}]$ response patterns change from sinusoidal oscillation to baseline spiking (Aa). The model predicts very similar behavior (Aa versus A1, Ab versus A2 and Ac versus A3). The transitions of the $[\text{Ca}_i^{2+}]$ response patterns are indicated on the bifurcation diagram ($k_{PK^*} \times k_p$) in (B). (C)–(Nash): When a cell is treated with a PKC inhibitor $[\text{Ca}_i^{2+}]$ oscillations change to TP-type response [57]. The cell with TP response due to pretreated PKC inhibitor recovered its $[\text{Ca}_i^{2+}]$ oscillation when the applied glutamate concentration was reduced. The model reproduces the same pattern, and positions of the type of $[\text{Ca}_i^{2+}]$ responses are identified on the bifurcation diagram on $k_{PK^*} \times L$ (C). As PKC activity is lowered, the system moves out of oscillatory region (SO)→(TP) and it reenters oscillatory region as L decreases (TP)→(BS). (D) The bifurcation diagram using $k_{PK^*} \times L$ is compared with that using $k_{PK^*} \times k_p$.

we constructed a bifurcation diagram using the parameters for PKC activity (k_{PK^*}) and glutamate concentration (L) in figure 7(D). Because IP_3 production is proportional to glutamate concentration, the two-parameter diagrams in $k_{PK^*} \times k_p$ and $k_{PK^*} \times L$ share similar features, as stated previously, including separation of four different $[\text{Ca}_i^{2+}]$ response patterns (7(D)). The two-parameter diagram in $k_{PK^*} \times L$ shows that the model also reproduces the same result, and in addition, the bifurcation diagram of PKC activity versus glutamate concentration reveals a possible mechanism underlying the observation by Nash *et al.* When PKC activity is inhibited with glutamate concentration fixed, the system moves from the sinusoidal oscillation region to a transient with plateau region (figures 4(C1) and

7(C)-(SO)→(TP)) and it reenters the oscillatory region as glutamate concentration decreases (figures 4(C1) and 7(C)-(TP)→(BS)).

Figure 3(C) shows how the level of $[\text{PKC}^*]_{ss}$ depends on the interaction of the amplifying module (k_p) and the feedback module (k_{PK^*}). Also, we see that the $[\text{PKC}^*]_{ss}$ level does not always coincide with a specific type of Ca_i^{2+} response pattern (compare between figures 3(C) and 4(A)). For example, the level of $[\text{PKC}^*]_{ss}$ in the BLS region at higher k_{PK^*} , may be larger than that in the TP region at lower k_{PK^*} . Therefore, knowing the absolute level of PKC^* is insufficient to determine the Ca_i^{2+} response type; both PLC^* and PKC^* activity have to be considered.

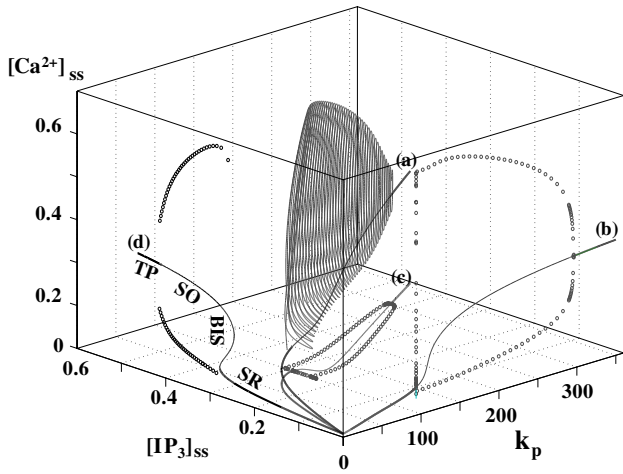


Figure 8. The steady states of $[IP_3]$ and $[Ca_i^{2+}]$ as a function of k_p for $k_{PK^*} = 1$. (a) Static and periodic solutions of $[IP_3]$ and $[Ca_i^{2+}]$ with respect to k_p are plotted in $k_p \times [IP_3]_{ss} \times [Ca_i^{2+}]_{ss}$ space. (b) The projection of (a) to $[IP_3] = 0$ plane (figure 4(B)). (c) The projection of (a) to $[IP_3] = 0$ plane (figure 4(C)). (d) The projection of (a) to $k_p = 0$ plane. The four different Ca_i^{2+} response patterns in (b) and (c), are labeled in (d). For different k_{PK^*} , the shapes of (b) and (c) may differ, but the projections on $[IP_3]_{ss} \times [Ca_i^{2+}]_{ss}$ are qualitatively similar to (d).

3.4. The relationship between cytosolic $[IP_3]$ levels and the $[Ca_i^{2+}]$ response patterns

Nash *et al* [57] proposed that $[IP_3]$ is responsible for the different types of Ca_i^{2+} responses, while in previous sections we have seen that the cooperative interaction of PKC and PLC is responsible for various $[Ca_i^{2+}]$ response patterns. Because both PKC and PLC participate in controlling cytosolic $[IP_3]$, $[IP_3]$ may play a crucial role in the different $[Ca_i^{2+}]$ response patterns, including the two distinct $[Ca_i^{2+}]$ oscillatory patterns. To study how the $[IP_3]$ level influences the $[Ca_i^{2+}]$ response patterns, the steady-state values of $[IP_3]$ and $[Ca_i^{2+}]$ have been replotted as a function of the PLC activity level (k_p) at a fixed PKC activity ($k_{PK^*} = 1$) in figure 8; the curves for other values are similar. A similar plot could be made as a function of PKC activity, but this is not done here. The static and periodic solutions of $[IP_3]$ and $[Ca_i^{2+}]$ are shown as the curve in figure 8(a), and from this curve one obtains the projections onto the various coordinate planes shown in figure 8.

The fact that the four different types of Ca_i^{2+} response patterns are possible even at zero PKC activity suggests that they originate in the output module, and that the role of the other modules is to modulate the IP_3 level in response to a broad spectrum of external signaling. To further investigate this, we have isolated output module (equations (17)–(20)) with $[IP_3]$ as a parameter and studied its behaviors by varying the 3R inactivation rate (k_{RCC} and k_{-RCC}). By choosing $(k_{RCC}, k_{-RCC}) = (0.9, 1.12)$, $(k_{RCC}, k_{-RCC}) = (1.8, 0.21)$ and $(k_{RCC}, k_{-RCC}) = (4.0, 0.2)$, it is possible to construct models (figure 9) which show only BLS-type Ca_i^{2+} oscillation (BLS model), both BLS and SO types Ca_i^{2+} oscillation (Mixed model) and only SO-type Ca_i^{2+} oscillation (SO model).

We compared the $([IP_3]_{ss}(k_p), [Ca_i^{2+}]_{ss}(k_p))$ curve with the static bifurcation diagram of the output module with $[IP_3]$ as a control parameter and found that these are also identical (figures 8(d) and 9(B1)). Recall that the model shows BLS starting at $[IP_3]_{ss} \simeq 0.278$ (figure 3(B1)-(b)) until it hits the local minimum and rises to $[IP_3]_{ss} \simeq 0.278$ (figures 3(B1)-(b), 8(b) and 4(A)) where the rate of change in $[IP_3]_{ss}$ with respect to k_p is small. If we identify figure 4(A)-(b) as the end point of BLS-type Ca_i^{2+} response, we also can compute the corresponding $[Ca_i^{2+}]_{ss}$ value at which BLS ends and OS begins on $([IP_3]_{ss}(k_p), [Ca_i^{2+}]_{ss}(k_p))$ curve in figure 8(d), which is approximately $[Ca_i^{2+}]_{ss} \simeq 0.21$ (μM). With the information in figure 4(A), it is possible to separate SR, BLS, OS and TP by $[Ca_i^{2+}]_{ss}$ regardless of strength of PKC and PLC activities: SR in $(0, 0.064)$, BLS in $[0.064, 0.21)$, SO in $[0.21, 0.26)$ and TP in $(0.26, \infty)$. Based on this observation, we may use $[Ca_i^{2+}]_{ss}(k_p)$ as an indicator of Ca_i^{2+} response patterns (figure 8(d)).

Tang and Othmer [83] showed that Ca_i^{2+} signaling in the CICR model can be frequency encoding, which is a major characteristic of BLS. To quantify the change in frequency in each model, we define the frequency quotient (FQ) as the ratio of the maximal and minimal frequency of a periodic solution over oscillatory region of $[IP_3]$. Similarly, to quantify the change in amplitude in each model, we define an amplitude quotient (AQ) as the fraction of maximal and minimal amplitudes of a periodic solution over the oscillatory region of $[IP_3]$. As found in other studies (table 1), the BLS model shows a wide range of frequency and period (figures 9(A2) and (A3)), while its amplitudes are relatively constant (figure 9(B1)), implying frequency-encoded signaling pattern by $[IP_3]$. For the BLS model, AQ is found to be 1.4, while FQ is ∞ the period is infinite at the first bifurcation point. To obtain frequency encoding of the BLS model directly, we set $[IP_3]$ at 0.28 and 0.5 (μM) in figure 9(A4) and (A5), respectively, where one sees that the change in frequency is very large but the amplitude change is small.

On the other hand, the SO model shows a large difference in amplitudes (figure 9(C1)), while relatively small changes in frequency and period are observed (figures 9(C2) and (C3)). Figures 9(C4) and (C5) with $[IP_3] = 0.45$ and 0.65 (μM) show the increase in amplitude at higher $[IP_3]$ in SO. Opposite to the BLS model, FQ is approximately 1.5 and AQ is ∞ (Zero minimal amplitude), indicating amplitude-encoded signaling pattern by $[IP_3]$. The mixed model (figure 9(B)) was generated by parameter values used in the full model (equations (7)–(25)), and four different modes of Ca_i^{2+} responses are possible depending on $[IP_3]$. In this case, both AQ and FQ are . The frequency and period profile of the mixed model (figures 9(B2) and (B3)) indicate that there exist frequency sensitive and insensitive regions in the range of $[IP_3]$. For lower $[IP_3]$ frequency encoding is prominent, while the change in period and frequency decreases as $[IP_3]$ increases. As seen in the previous section, the mixed model reveals BLS at lower $[IP_3]$ (figure 9(B4): $[IP_3] = 0.279 \mu M$) and SO at higher $[IP_3]$ (figure 9(B4): $[IP_3] = 0.45 \mu M$).

In some studies [56, 57], the type of the GPCR was regarded as a major determinant of the Ca_i^{2+} response type.

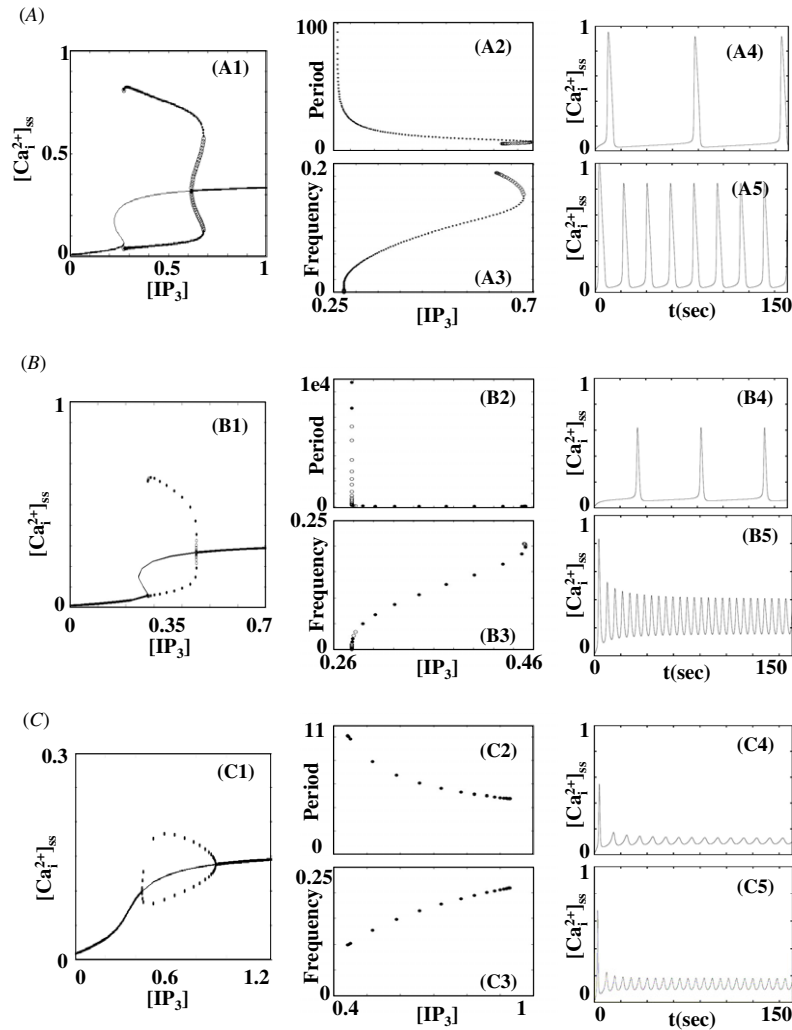


Figure 9. Prototype models of different Ca_i^{2+} oscillation (A): A model showing only BLS type Ca_i^{2+} response ($k_{RCC} = 0.9, k_{-RCC} = 0.12$). (B): A model showing four different type Ca_i^{2+} responses ($k_{RCC} = 1.8, k_{-RCC} = 0.21$). (C): A model showing only SO-type Ca_i^{2+} response ($k_{RCC} = 4, k_{-RCC} = 0.2$). (A1), (B1) & (C1): Bifurcation diagram of static and periodic solution with $[\text{IP}_3]$ as a control parameter. (A2), (B2) and (C2): Periods of periodic solutions. (A3), (B3) and (C3): Frequency of periodic solutions. (A4), (B4) and (C4): Time course of periodic solution at lower $[\text{IP}_3]$. (A5), (B5) and (C5): Time course of periodic solution at higher $[\text{IP}_3]$. For (A4, B4, C4), $[\text{IP}_3] = (0.28, 0.279, 0.45)$ was used and for (A5, B5, C5), $[\text{IP}_3] = (0.5, 0.45, 0.65)$ was used. (A)–(C) indicates that different Ca_i^{2+} response pattern may come from time scale of IP_3R inactivation by high $[\text{Ca}_i^{2+}]$ rather (or biphasic profile of IP_3R gated channel open probability) than specific ligand receptor on plasma membrane.

However, figure 9 leaves open the possibility that the time scale of inactivation of IP_3R by Ca_i^{2+} may cause different Ca_i^{2+} response types. In particular, for cells in which BLS is dominant, we suggest that the time scale of inactivation of IP_3R by Ca_i^{2+} (figure 9(A); $k_{RCC} = 0.9, k_{-RCC} = 1.12$) is slower than that of cells that show four different Ca_i^{2+} response types (figure 9(A); $k_{RCC} = 1.8, k_{-RCC} = 0.21$).

4. Conclusion and outlook

Many cells can show various and complex Ca_i^{2+} responses to many extracellular stimuli by mobilizing the stored Ca^{2+} in the ER. These responses can be both temporal and spatial and usually the temporal and spatial patterns of Ca^{2+} are

very diverse and complex. In spite of the diversity, temporal Ca_i^{2+} responses under sustained agonist stimulus fall into some typical categories: (i) subthreshold Ca^{2+} response, (ii) baseline spiking, (iii) sinusoidal oscillation, and (iv) transient Ca^{2+} spike with plateau. Although many studies indicated that inhibition of both ligand receptors and PLC by PKC is responsible for SO, while a PKC-independent CICR mechanism is believed to be responsible for BLS, our results suggest that the strength of PKC activity is not a sufficient criterion to define BLS and SO: both baseline spiking and sinusoidal oscillations can be observed as PLC activity varies regardless of PKC activity, even at zero PKC activity. We have shown that the $[\text{IP}_3]$ level due to PLC and PKC activities can be regarded as a factor that determines Ca_i^{2+} response patterns. LeBeau *et al* [48] reported that a different type of IP_3R gated channel that has

a different opening probability as a function of $[IP_3]$ shows different $[Ca_i^{2+}]$ oscillation patterns, which is compatible with our conclusion.

As we have seen, there are observable differences between BLS and SO. Firstly, SO exhibits rather high-frequency sustained oscillations of slowly-decreasing amplitude above the basal $[Ca_i^{2+}]$ level, while BLS is characterized by $[IP_3]$ -independent, constant-amplitude spiking starting from a low basal level and a low frequency. The differences of $[Ca_i^{2+}]$ levels from which $[Ca_i^{2+}]$ oscillations originate stem from the $[IP_3]$ level, because $[IP_3]$ and $[Ca_i^{2+}]$ are approximately proportional to each other. The balance of PKC and PLC activities are important to maintain the intracellular $[Ca_i^{2+}]$ oscillation; sufficient imbalance of these two activities results in non-oscillatory responses. When PKC activity is dominant over PLC activity, SR is expected while when PLC activity is dominant, TP-type Ca^{2+} response pattern is observed due to excessive IP_3 saturating IP_3RS . When PKC and PLC activities were balanced, the oscillatory Ca^{2+} response is observed. Since the BLS is observed at comparatively low activity of PLC inducing low levels of $[IP_3]$, DAG, and Ca^{2+} , PKC level are also low, and a long period of latency is observed before the first high amplitude of spike. Some characteristics of two different types of $[Ca_i^{2+}]$ oscillation patterns are compared in table 1.

It is known that BLS is the only type of Ca_i^{2+} response in some cell types, while in others, including astrocytes, four different types of Ca_i^{2+} responses can be observed. Our model suggests either that there are additional mechanisms that maintain $[IP_3]$ at a certain level, or that the time scale of inactivation of the IP_3R -gated Ca^{2+} channel is relatively slow in cells that exhibit only the BLS type of Ca_i^{2+} response.

Certainly many factors, in addition to those considered here, can affect the type of oscillation, including the agonist type and concentration [48, 57, 64], the receptor type and concentration [56, 57, 64], IP_3 and IP_3R [47, 48, 100], cytosolic proteins and buffers [50, 64] and the mitochondria [32, 50, 51]. In the case of excitable cells, the membrane potential also plays a role [37, 38]. Furthermore, it is not clear how important stochastic effects are in setting the patterns of calcium response. The dynamics of individual channels is certainly stochastic, but whether this is important at the whole-cell level depends on the context. When Ca_i^{2+} release is highly localized spatial effects may be important and the situation is more complex. For example, it has been shown that changes in the average cluster spacing can generate different $[Ca_i^{2+}]$ response patterns independent of stimulation strength [25, 26]. Recently, integrations of both deterministic and stochastic aspects have been incorporated into either multiscale descriptions or hybrid models [46, 69].

In addition to temporal patterns of Ca^{2+} responses, spatial patterns or waves also have important physiological implications. In general, while localized Ca^{2+} events are believed to have roles in local events such as exocytosis [89], spatial Ca^{2+} waves can be used as a global signaling mechanism. Ca^{2+} waves can propagate through the cytoplasm of a single cell or even multiple cells, activating distal Ca^{2+} sensing targets, as observed, for example in the fertilization

of oocytes [95]. In the latter case the local dynamics are excitable and waves may propagate for millimeters, even though diffusion alone is not effective on this scale [11, 18, 62]. Ca^{2+} waves through multiple cells have been observed in ciliated airway epithelial cells [9], pancreatic acinar cells [79], hepatocytes in the liver [71], as well as in the astrocyte network [12]. In Ca^{2+} signaling between connected homogeneous cells, each cell is assumed to have the same intracellular kinetic parameters that characterize intracellular Ca^{2+} mobilization. However, it is expected that there are $[IP_3]$ differences between a directly-stimulated cell and other neighboring cells receiving the Ca^{2+} signal indirectly by either Ca^{2+} or IP_3 diffusion, because Ca^{2+} waves are confined within finite distance (Otherwise Ca^{2+} wave propagate forever). Because the $[IP_3]$ level directly determines the type of $[Ca_i^{2+}]$ response patterns, it is also expected that there is transition from one type of $[Ca_i^{2+}]$ response pattern to another $[Ca_i^{2+}]$ response pattern as Ca^{2+} waves propagate. For example, a group of directly-stimulated cells may show a TP-type response, neighboring cells may show SO or BLS, depending on the distance from the stimulated cells, and the Ca^{2+} waves may terminate in distal cells where the SR response is dominant. It is not known how the different $[Ca_i^{2+}]$ response patterns contribute in cellular signaling, but the current study suggests that $[Ca_i^{2+}]$ signaling patterns may be more complex when both temporal and spatial aspects are involved.

Glossary

<i>AMPA</i>	alpha-amino-3-hydroxy-5-methyl-4-isoxazolepropionic acid
<i>AQ</i>	amplitude quotient
<i>BLS</i>	baseline spiking
<i>CICR</i>	Ca^{2+} -induced Ca^{2+} release
<i>DAG</i>	diacylglycerol
<i>ER</i>	endoplasmic reticulum
<i>FQ</i>	frequency quotient
<i>GDP</i>	guanosine diphosphate
<i>GPCR</i>	G protein-coupled receptor
<i>GTP</i>	guanosine triphosphate
IP_3	inositol trisphosphate
<i>mGluR</i>	metabotropic glutamate receptor
<i>NMDA</i>	N-methyl-D-aspartic acid
<i>PDBu</i>	phorbol 12,13-dibutyrate
<i>PKC</i>	protein kinase C
<i>PLC</i>	phospholipase C
<i>SERCA</i>	sarco/endoplasmic reticulum Ca^{2+} -ATPase
<i>SO</i>	sinusoidal oscillations
<i>SR</i>	sub-threshold response
<i>TP</i>	transient with plateau

References

- [1] Bartlett P J, Young K W, Nahorski S R and John Challiss R A 2005 Single cell analysis and temporal profiling of agonist-mediated inositol 1,4,5-trisphosphate, Ca^{2+} , diacylglycerol, and protein kinase C signaling using fluorescent biosensors *J. Biol. Chem.* **280** 21837–46

- [2] Berridge M J 1990 Calcium oscillations *J. Biol. Chem.* **265** 9583–6
- [3] Berridge M J 1997 Elementary and global aspects of calcium signalling *J. Exp. Biol.* **200** 315–9
- [4] Berridge M J, Bootman M D and Lipp P 1998 Calcium—a life and death signal *Nature* **395** 645–8
- [5] Berstein G, Blank J L, Jhon D Y, Exton J H, Rhee S G and Ross E M 1992 Phospholipase c-beta 1 is a gtpase-activating protein for gq/11, its physiologic regulator *Cell* **70** 411–8
- [6] Bezprozvanny I and Ehrlich B E 1995 The inositol 1,4,5-trisphosphate (insp3) receptor *J. Membr. Biol.* **145** 205–16
- [7] Bhalla U S and Iyengar R 1999 Emergent properties of networks of biological signaling pathways *Science* **283** 381–7
- [8] Bird G S, Rossier M F, Obie J F and Putney J W 1993 Sinusoidal oscillations in intracellular calcium requiring negative feedback by protein kinase c *J. Biol. Chem.* **268** 8425–8
- [9] Boitano S, Dirksen E R and Sanderson M J 1992 Intercellular propagation of calcium waves mediated by inositol trisphosphate *Science* **258** 292–5
- [10] Borghans J M, Dupont G and Goldbeter A 1997 Complex intracellular calcium oscillations. a theoretical exploration of possible mechanisms *Biophys. Chem.* **66** 25–41
- [11] Callamaras N, Marchant J S, Sun X P and Parker I 1998 Activation and co-ordination of insp3-mediated elementary Ca^{2+} events during global Ca^{2+} signals in xenopus oocytes *J. Physiol.* **509** 81–91
- [12] Charles A 2005 Reaching out beyond the synapse: glial intercellular waves coordinate metabolism *STKE* **2005** pe6
- [13] Clements J D, Lester R A, Tong G, Jahr C E and Westbrook G L 1992 The time course of glutamate in the synaptic cleft *Science* **258** 1498–501
- [14] Codazzi F, Teruel M N and Meyer T 2001 Control of astrocyte $Ca(2+)$ oscillations and waves by oscillating translocation and activation of protein kinase c *Curr. Biol.* **11** 1089–97
- [15] Cornell-Bell A H and Finkbeiner S M 1991 Ca^{2+} waves in astrocytes *Cell Calcium* **12** 185–204
- [16] da Silva C P and Guse A H 2000 Intracellular $Ca(2+)$ release mechanisms: multiple pathways having multiple functions within the same cell type? *Biochim. Biophys. Acta* **1498** 122–33
- [17] Dale L B, Babwah A V, Bhattacharya M, Kelvin D J and Ferguson S S 2001 Spatial-temporal patterning of metabotropic glutamate receptor-mediated inositol 1,4,5-trisphosphate, calcium, and protein kinase c oscillations: protein kinase c-dependent receptor phosphorylation is not required *J. Biol. Chem.* **276** 35900–8
- [18] Dargan S L and Parker Ian 2003 Buffer kinetics shape the spatiotemporal patterns of ip3-evoked $Ca(2+)$ signals *J. Physiol.* **553** 775–88
- [19] Dolmetsch R E, Xu K and Lewis R S 1998 Calcium oscillations increase the efficiency and specificity of gene expression *Nature* **392** 933–6
- [20] DOQCS 2003 The database of quantitative cellular signaling. <http://doqcs.ncbs.res.in>
- [21] Dupont G and Swillens S 1996 Quantal release, incremental detection, and long-period $Ca(2+)$ oscillations in a model based on regulatory $Ca(2+)$ -binding sites along the permeation pathway *Biophys. J.* **71** 1714–22
- [22] Dupont G, Swillens S, Clair C, Tordjmann T and Combettes L 2000 Hierarchical organization of calcium signals in hepatocytes: from experiments to models *Biochim. Biophys. Acta* **1498** 134–52
- [23] Dupont G, Combettes L and Leybaert L 2007 Calcium dynamics: spatio-temporal organization from the subcellular to the organ level *Int. Rev. Cytol.* **261** 193–245
- [24] East J M 2000 Sarco (endo)plasmic reticulum calcium pumps recent advances in our understanding of structure/function and biology (review) *Mol. Membr. Biol.* **17** 189–200
- [25] Falcke M 2003 On the role of stochastic channel behavior in intracellular Ca^{2+} dynamics *Biophys. J.* **84** 42–56
- [26] Falcke Martin 2004 Reading the patterns in living cells—the physics of Ca^{2+} signaling *Adv. Phys.* **53** 255–440
- [27] Fay S P, Posner R G, Swann W N and Sklar L A 1991 Real-time analysis of the assembly of ligand, receptor, and g protein by quantitative fluorescence flow cytometry *Biochemistry* **30** 5066–75
- [28] Fiacco T A and McCarthy K D 2006 Astrocyte calcium elevations: properties, propagation, and effects on brain signaling *Glia* **54** 676–90
- [29] Filtz T M, Cunningham M L, Stanig K J, Paterson A and Harden T K 1999 Phosphorylation by protein kinase c decreases catalytic activity of avian phospholipase c-beta *Biochem. J.* **338** 257–64
- [30] Francesconi A and Duvoisin R M 2000 Opposing effects of protein kinase c and protein kinase a on metabotropic glutamate receptor signaling: selective desensitization of the inositol trisphosphate/ Ca^{2+} pathway by phosphorylation of the receptor-g protein-coupling domain *Proc. Natl Acad. Sci. USA* **97** 6185–90
- [31] Gallegos L L, Kunkel M T and Newton A C 2006 Targeting protein kinase c activity reporter to discrete intracellular regions reveals spatiotemporal differences in agonist-dependent signaling *J. Biol. Chem.* **281** 30947–56
- [32] Grubelnik V, Larsen A Z, Kummer U, Olsen L F and Marhl M 2001 Mitochondria regulate the amplitude of simple and complex calcium oscillations *Biophys. Chem.* **94** 59–74
- [33] Harootunian A T, Kao J P, Paranjape S and Tsien R Y 1991 Generation of calcium oscillations in fibroblasts by positive feedback between calcium and ip3 *Science* **251** 75–8
- [34] Homma Y, Imaki J, Nakanishi O and Takenawa T 1988 Isolation and characterization of two different forms of inositol phospholipid-specific phospholipase c from rat brain *J. Biol. Chem.* **263** 6592–8
- [35] Houart G, Dupont G and Goldbeter A 1999 Bursting, chaos and birhythmicity originating from self-modulation of the inositol 1,4,5-trisphosphate signal in a model for intracellular Ca^{2+} oscillations *Bull. Math. Biol.* **61** 507–30
- [36] Jacob R 1990 Calcium oscillations in electrically non-excitable cells *Biochim. Biophys. Acta* **1052** 427–38
- [37] Jafri M S and Gillo B 1994 A membrane potential model with counterions for cytosolic calcium oscillations *Cell Calcium* **16** 9–19
- [38] Jafri M S, Vajda S, Pasik P and Gillo B 1992 A membrane model for cytosolic calcium oscillations. a study using xenopus oocytes *Biophys. J.* **63** 235–46
- [39] Joseph S K 1996 The inositol triphosphate receptor family *Cell Signal* **8** 1–7
- [40] Kato M, Doi R, Imamura M, Okada N, Shimada Y, Hosotani R and Miyazaki J I 1998 Response of human insulinoma cells to extracellular calcium is different from normal b cells *Dig. Dis. Sci.* **43** 2429–38
- [41] Kawabata S, Tsutsumi R, Kohara A, Yamaguchi T, Nakanishi S and Okada M 1996 Control of calcium oscillations by phosphorylation of metabotropic glutamate receptors *Nature* **383** 89–92
- [42] Keizer J and De Young G W 1992 Two roles of Ca^{2+} in agonist stimulated Ca^{2+} oscillations *Biophys. J.* **61** 649–80
- [43] Kim W T, Rioult M G and Cornell-Bell A H 1994 Glutamate-induced calcium signaling in astrocytes *Glia* **11** 173–84

- [44] De Koninck P and Schulman H 1998 Sensitivity of cam kinase ii to the frequency of Ca^{2+} oscillations *Science* **279** 227–30
- [45] Kummer U, Olsen L F, Dixon C J, Green A K, Bornberg-Bauer E and Baier G 2000 Switching from simple to complex oscillations in calcium signaling *Biophys. J.* **79** 1188–95
- [46] Kummer U, Krajnc B, Pahle J, Green A K, Dixon C J and Marhl M 2005 Transition from stochastic to deterministic behavior in calcium oscillations *Biophys. J.* **89** 1603–11
- [47] Lawrie A M, Toescu E C and Gallacher D V 1993 Two different spatiotemporal patterns for Ca^{2+} oscillations in pancreatic acinar cells: evidence of a role for protein kinase c in ins(1,4,5)p3-mediated Ca^{2+} signalling *Cell Calcium* **14** 698–710
- [48] LeBeau A P, Yule D I, Groblewski G E and Sneyd J 1999 Agonist-dependent phosphorylation of the inositol 1,4,5-trisphosphate receptor: a possible mechanism for agonist-specific calcium oscillations in pancreatic acinar cells *J. Gen. Physiol.* **113** 851–72
- [49] Li W, Llopis J, Whitney M, Zlokarnik G and Tsien R Y 1998 Cell-permeant caged inositol 3 ester shows that Ca^{2+} spike frequency can optimize gene expression *Nature* **392** 936–41
- [50] Marhl M, Haberichter T, Brumen M and Heinrich R 2000 Complex calcium oscillations and the role of mitochondria and cytosolic proteins *Biosystems* **57** 75–86
- [51] Marhl M, Schuster S and Brumen M 1998 Mitochondria as an important factor in the maintenance of constant amplitudes of cytosolic calcium oscillations *Biophys. Chem.* **71** 125–32
- [52] McLaughlin S, Wang J, Gambhir A and Murray D 2002 Pip(2) and proteins: interactions, organization, and information flow *Annu. Rev. Biophys. Biomol. Struct.* **31** 151–75
- [53] Mikoshiba K and Hattori M 2000 IP_3 receptor-operated calcium entry *STKE* **2000** pe1
- [54] Mishra J and Bhalla U S 2002 Simulations of inositol phosphate metabolism and its interaction with inositol(3)-mediated calcium release *Biophys. J.* **83** 1298–316
- [55] Nakahara K, Okada M and Nakanishi S 1997 The metabotropic glutamate receptor mglur5 induces calcium oscillations in cultured astrocytes via protein kinase c phosphorylation *J. Neurochem.* **69** 1467–75
- [56] Nash M S, Young K W, Challiss R A and Nahorski S R 2001 Intracellular signalling. receptor-specific messenger oscillations *Nature* **413** 381–2
- [57] Nash M S, Schell M J, Atkinson P J, Johnston N R, Nahorski S R and John Challiss R A 2002 Determinants of metabotropic glutamate receptor-5-mediated $\text{Ca}(2+)$ and inositol 1,4,5-trisphosphate oscillation frequency. receptor density versus agonist concentration *J. Biol. Chem.* **277** 35947–60
- [58] Nicoletti F, Iadarola M J, Wroblewski J T and Costa E 1986 Excitatory amino acid recognition sites coupled with inositol phospholipid metabolism: developmental changes and interaction with alpha 1-adrenoceptors *Proc. Natl Acad. Sci. USA* **83** 1931–5
- [59] Othmer H and Tang Y 1993 Oscillations and waves in a model of InsP3-controlled calcium dynamics *Experimental and theoretical Advances in Biological Pattern Formations* (New York: Plenum)
- [60] Palmer R K, Yule D I, McEwen E L, Williams J A and Fisher S K 1994 Agonist-specific calcium signaling and phosphoinositide hydrolysis in human sk-n-mcixc neuroepithelioma cells *J. Neurochem.* **63** 2099–107
- [61] Pang I H and Sternweis P C 1990 Purification of unique alpha subunits of gtp-binding regulatory proteins (g proteins) by affinity chromatography with immobilized beta gamma subunits *J. Biol. Chem.* **265** 18707–12
- [62] Parker I and Yao Y 1991 Regenerative release of calcium from functionally discrete subcellular stores by inositol trisphosphate *Proc. Biol. Sci.* **246** 269–74
- [63] Periasamy M and Kalyanasundaram A 2007 Serca pump isoforms: their role in calcium transport and disease *Muscle Nerve* **35** 430–42
- [64] Petersen C C, Toescu E C and Petersen O H 1991 Different patterns of receptor-activated cytoplasmic Ca^{2+} oscillations in single pancreatic acinar cells: dependence on receptor type, agonist concentration and intracellular Ca^{2+} buffering *EMBO J.* **10** 527–33
- [65] Prentki M, Glennon M C, Thomas A P, Morris R L, Matschinsky F M and Corkey B E 1988 Cell-specific patterns of oscillating free $\text{Ca}(2+)$ in carbamylcholine-stimulated insulinoma cells *J. Biol. Chem.* **263** 11044–7
- [66] Putney J W and Bird G S 1993 The inositol phosphate-calcium signaling system in nonexcitable cells *Endocr. Rev.* **14** 610–31
- [67] Putney J W Jr 1997 *Capacitative Calcium Entry* (Austin, TX: Landes Biomedical Publishing)
- [68] Putney J W 1998 *Basic Neurochemistry: Molecular, Cellular and Medical Aspects chapter Calcium* (Philadelphia, PA: Lippincott Williams and Wilkins) pp 453–70
- [69] Rüdiger S, Shuai J W, Huisinga W, Nagaiah C, Warnecke G, Parker I and Falcke M 2007 Hybrid stochastic and deterministic simulations of calcium blips *Biophys. J.* **93** 1847–57
- [70] Rink T J and Merritt J E 1990 Calcium signalling *Curr. Opin. Cell Biol.* **2** 198–205
- [71] Robb-Gaspers L D and Thomas A P 1995 Coordination of $\text{Ca}(2+)$ signaling by intercellular propagation of $\text{Ca}(2+)$ waves in the intact liver *J. Biol. Chem.* **270** 8102–7
- [72] Rooney T A, Sass E J and Thomas A P 1989 Characterization of cytosolic calcium oscillations induced by phenylephrine and vasopressin in single fura-2-loaded hepatocytes *J. Biol. Chem.* **264** 17131–41
- [73] Rosay P, Davies S A, Yu Y, Sözen A, Kaiser K and Dow J A 1997 Cell-type specific calcium signalling in a drosophila epithelium *J. Cell Sci.* **110** 1683–92
- [74] Savineau J-P and Marthan R 2000 Cytosolic calcium oscillations in smooth muscle cells *News Physiol. Sci.* **15** 50–5
- [75] Schaefer M, Mischak H, Schnell S, Griese A, Iakubov R, Riepenhausen G and Schoff C 2004 Mechanisms of arginine-vasopressin-induced Ca^{2+} oscillations in beta-cells (hit-t15): a role for oscillating protein kinase c *Endocrinology* **145** 4635–44
- [76] Schuster S, Marhl M and Höfer T 2002 Modelling of simple and complex calcium oscillations. from single-cell responses to intercellular signalling *Eur. J. Biochem.* **269** 1333–55
- [77] Sneyd J, Keizer J and Sanderson M J 1995 Mechanisms of calcium oscillations and waves: a quantitative analysis *FASEB J.* **9** 1463–72
- [78] Soto G and Othmer H G 2006 A model for a g-protein-mediated mechanism for synaptic channel modulation *Math Biosci.* **200** 188–213
- [79] Stauffer P L, Zhao H, Luby-Phelps K, Moss R L, Star R A and Muallem S 1993 Gap junction communication modulates $[\text{Ca}^{2+}]_i$ oscillations and enzyme secretion in pancreatic acini *J. Biol. Chem.* **268** 19769–75
- [80] Strahonja-Packard A and Sanderson M J 1999 Intercellular $\text{Ca}(2+)$ waves induce temporally and spatially distinct intracellular $\text{Ca}(2+)$ oscillations in glia *Glia* **28** 97–113
- [81] Swillens S, Combettes L and Champeil P 1994 Transient inositol 1,4,5-trisphosphate-induced $\text{Ca}(2+)$ release: a model based on regulatory $\text{Ca}(2+)$ -binding sites along the

- permeation pathway *Proc. Natl Acad. Sci. USA* **91** 10074–8
- [82] Tang Y and Othmer H G 1994 A g protein-based model of adaptation in dictyostelium discoideum *Math. Biosci.* **120** 25–76
- [83] Tang Y and Othmer H G 1995 Frequency encoding in excitable systems with applications to calcium oscillations *Proc. Natl Acad. Sci. USA* **92** 7869–73
- [84] Tang Y, Stephenson J L and Othmer H G 1996 Simplification and analysis of models of calcium dynamics based on ip_3 -sensitive calcium channel kinetics *Biophys. J.* **70** 246–63
- [85] Tanimura A, Nezu A, Morita T, Hashimoto N and Tojyo Y 2002 Interplay between calcium, diacylglycerol, and phosphorylation in the spatial and temporal regulation of $\text{pk}\alpha$ -gfp *J. Biol. Chem.* **277** 29054–62
- [86] Taylor C W 1998 Inositol trisphosphate receptors: Ca^{2+} -modulated intracellular Ca^{2+} channels *Biochim. Biophys. Acta* **1436** 19–33
- [87] Taylor C W and Traynor D 1995 Calcium and inositol trisphosphate receptors *J. Membr. Biol.* **145** 109–18
- [88] Thomas A P, Bird G S, Hajnóczky G, Robb-Gaspers L D and Putney J W 1996 Spatial and temporal aspects of cellular calcium signaling *FASEB J.* **10** 1505–17
- [89] Thorn P, Lawrie A M, Smith P M, Gallacher D V and Petersen O H 1993 $\text{Ca}(2+)$ oscillations in pancreatic acinar cells: spatiotemporal relationships and functional implications *Cell Calcium* **14** 746–57
- [90] Tovey S C *et al* 2001 Calcium puffs are generic $\text{insp}(3)$ -activated elementary calcium signals and are downregulated by prolonged hormonal stimulation to inhibit cellular calcium responses *J. Cell Sci.* **114** 3979–89
- [91] Tsien R W and Tsien R Y 1990 Calcium channels, stores, and oscillations *Annu. Rev. Cell Biol.* **6** 715–60
- [92] Verkhratsky A and Toescu E C 2003 Endoplasmic reticulum $\text{Ca}(2+)$ homeostasis and neuronal death *J. Cell Mol. Med.* **7** 351–61
- [93] Violin J D and Newton A C 2003 Pathway illuminated: visualizing protein kinase c signaling *IUBMB Life* **55** 653–60
- [94] Violin J D, Zhang Jin, Tsien R Y and Newton A C 2003 A genetically encoded fluorescent reporter reveals oscillatory phosphorylation by protein kinase c *J. Cell Biol.* **161** 899–909
- [95] Whitaker M 2006 Calcium at fertilization and in early development *Physiol. Rev.* **86** 25–88
- [96] Wu Minnie M, Luik R M and Lewis R S 2007 Some assembly required: constructing the elementary units of store-operated Ca^{2+} entry *Cell Calcium* **42** 163–72
- [97] Chang Xu, Watras J and Loew L M 2003 Kinetic analysis of receptor-activated phosphoinositide turnover *J. Cell Biol.* **161** 779–91
- [98] Yoshida Y and Imai S 1997 Structure and function of inositol 1,4,5-trisphosphate receptor *Japan. J. Pharmacol.* **74** 125–37
- [99] De Young G W and Keizer J 1992 A single-pool inositol 1,4,5-trisphosphate-receptor-based model for agonist-stimulated oscillations in $\text{Ca}(2+)$ concentration *Proc. Natl Acad. Sci. USA* **89** 9895–9
- [100] Young K W, Nash M S, John Challiss R A and Nahorski S R 2003 Role of $\text{Ca}(2+)$ feedback on single cell inositol 1,4,5-trisphosphate oscillations mediated by g-protein-coupled receptors *J. Biol. Chem.* **278** 20753–60
- [101] Steven H, Young S, Wu V and and Rozengurt E 2002 $\text{Ca}(2+)$ -stimulated $\text{Ca}(2+)$ oscillations produced by the $\text{Ca}(2+)$ -sensing receptor require negative feedback by protein kinase c *J. Biol. Chem.* **277** 46871–6
- [102] Yue C, Ku C Y, Liu M, Simon M I and Sanborn B M 2000 Molecular mechanism of the inhibition of phospholipase c beta 3 by protein kinase c *J. Biol. Chem.* **275** 30220–5